The CQL3D Fokker-Planck Code

(reconstituted in editable form from

General Atomics Report GA-A20978, 1992)

R.W. Harvey & M.G. McCoy

January 22, 2015

Abstract

CQL3D is a general purpose computer code for modeling auxiliary heating in tokamaks. It calculates the radial distribution of 2D in momentum-space bounce-averaged, ion and electron distribution functions in toroidal geometry, consistent with deposition of rf and/or neutral beam injected power and a diffusive radial transport model. This calculation is carried out with an array of bounce-averaged Fokker-Planck (FP) solvers running on noncircular magnetic flux surfaces, giving the steady-state, toroidally-averaged distribution resulting from a balance between collisions, dc electric field, rf quasilinear diffusion, synchrotron radiation, neutral beam injection, and radial diffusion. CQL3D is coupled to ray-tracing codes for electron cyclotron, lower hybrid, and fast waves, to a neutral beam deposition code, and to a noncircular equilibrium code. We describe the code, providing expressions and methodology for calculation of the FP coefficients from each of the constituent processes, and give benchmark applications in order to validate the major components of the code.

Chapter 1

INTRODUCTION

A complete Fokker-Planck (FP) treatment of rf or neutral beam heating in tokamaks on time scales longer than the collisional time ($\tau_{\rm coll}$) generally requires solution of an equation which is at least two dimensions in momentum/velocity space and two dimensions in configuration space. That is, we assume the distribution functions of electrons and ions are independent of azimuthal velocity angle about the ambient magnetic field and of spatial toroidal angle in the symmetry direction of the tokamak, in accord with the usual situation $\omega_{\rm c}^{-1} \ll \tau_{\rm coll}$ where $\omega_{\rm c}$ is the gyrofrequency of the particles, and the time for achieving toroidal equilibrium on a flux surface is short compared to $\tau_{\rm coll}$ or the transport time.

An associated further reduction in dimensionality occurs in cases where the bounce/transit time of the particles, $\tau_{\rm b}$, is short compared to the collision time, $\tau_{\rm b} \ll \tau_{\rm coll}$. The present generation of larger tokamak experimental devices *often* operate with most of the plasma in this low-collisionality "banana" regime. Moreover it is *usually* the case that the non-Maxwellian particles generated by auxiliary heating and current drive are in the low-collisionality regime. In such cases, a "bounce-average" over the bounce or toroidal transit motion of the particle is appropriate, reducing the FP equation to be essentially three-dimensional since the particle distributions as a function of poloidal angle become constant when expressed as a function of the collisionless constants of motion. We take the resulting three variables to be the magnitude u of the momentum-per-rest-mass, the pitch angle θ_0 measured from the magnetic field direction and evaluated at the minimum magnetic field position on a flux surface, and a radial coordinate ρ. These coordinates are independent variables for the three-dimensional bounce-averaged FP code CQL3D (Collisional QuasiLinear 3 D) which is the focus of this paper. Our purpose in this paper is to describe the code in detail and to validate it through several important benchmark applications in tokamak plasmas.

The CQL3D code, which had its genesis in the CQL code [1], consists of a 2 D-in-momentum-space, multi-species, relativistic, bounce-averaged, collisional/quasilinear FP equation solver running on a radial array of non-circular flux surfaces, in tandem with rf ray-tracing and/or neutral beam deposition packages. Sources in the FP equation resulting from the auxiliary heating systems, and concomitant self-consistent non-Maxwellian distortion of the distribution functions, are obtained. Radial transport is

accounted for by inclusion of radial diffusion and particle pinch operators. Thus, the code provides for transport of the full distribution functions. In comparison with the present generation of transport codes, the code transports all the moments of the distribution function rather than three moments (density, energy, and toroidal momentum); however CQL3D does not presently provide for a self-consistent solution with the time-dependent Ampère/Faraday laws. The code is similar to the BANDIT3D [2, 3], Giruzzi[4], Hammett[5], Fukuyama[6], and Smirnov[7] codes, but is different with regard to: greater generality, being multispecies, larger number of coupled deposition packages, noncircularity, and in other ways, including aspects of the numerical approach.

The methodology for obtaining the bounce-averaged, quasilinear rf FP coefficients due to combined Landau, transit-time, and cyclotron wave-particle interaction is new, and is discussed at length. Synchrotron radiation is strongly enhanced by electron nonthermal effect, and we describe our model for this process. The radial transport contains novel features which are described.

We consider the following four applications of the code. These applications mainly are to benchmark the code but also to elucidate the breadth of application possible with the code. Results [8] for banana-regime Ohmic conductivity both at low and high inverse aspect ratio ε accurately agree with previous analytic calculations. Good agreement is obtained between electron cyclotron damping calculated via the rf quasilinear operator in the code and a relativistic dispersion relation solver. Neutral beam current drive in an ITER-like plasma is calculated. Good agreement for current drive is found between a full multispecies (ion/electron) treatment of the particle distributions, and a FP code solution for only the ion distribution combined with an approximate analytic calculation of the electron contribution to NBCD. We also illustrate spreading of the runaway electrons by radial transport in a typical tokamak situation.

Chapter 2

FOKKER-PLANCK EQUATION

The theory of bounce-averaged FP equations for plasmas is examined in Refs. [1], [8], and [9]. Here we present a heuristic derivation of the appropriate bounce-averaged FP equation in order to review some of the underlying assumptions, to give notation, and to present the specific physical effects which are included in our treatment. The following section will provide greater detail on each of the terms in the equation.

We are interested in time scales of order or greater than the collision time; in usual tokamak situations this time is much greater than the cyclotron period of the electrons or ions. Thus, we assume the electron or ion distributions are azimuthally symmetric about the ambient magnetic field direction. In this "drift-kinetic" regime, we may take the particle distribution (more precisely, phase-space distribution of guiding centers) to be a function $f(\underline{r},\varepsilon,\mu,t)$ [10, 11, 12] where $\underline{r}$ is position vector, $\varepsilon=(\gamma-1)mc^2$ is particle kinetic energy, and $\mu=\frac{1}{2}u_\perp^2/B$ is magnetic moment. Here, γ is the relativistic factor $\gamma^2=1+u^2/c^2$, m is particle rest mass, c is the velocity of light, $\underline{u}=\underline{p}/m$ is particle momentum per mass, and B is the magnetic field strength. [13, 10, 11, 12] Subscripts indicating parallel and perpendicular refer to the magnetic field direction. Then the drift kinetic equation at each point $\underline{r}$ in the plasma can be written

$$\frac{df}{dt} = -\nabla_{\underline{u}}\cdot\Gamma_{\underline{u}}+R(f)+S, \tag{2.1}$$

where

$$\begin{aligned}\frac{df}{dt} &= \text{total derivative following the particle guiding center,}\\ &= \frac{\partial f}{\partial t}+\underline{v}_{\text{g.c.}}\cdot\frac{\partial f}{\partial \underline{r}}+\frac{\partial f}{\partial\mu}\frac{d\mu}{dt}+\frac{\partial f}{\partial\varepsilon}\frac{d\varepsilon}{dt},\end{aligned} \tag{2.2}$$

$$v_{\text{g.c.}} = v_\parallel\hat{b}+\vec{v}_{\text{D}},$$

$$\begin{aligned} \vec{v}_{\rm D} &= \text{guiding center drift perpendicular to } \hat{b} \equiv \underline{B}/B, \\ -\nabla_{\underline{u}} \cdot \underline{\Gamma}_{\underline{u}} &= C(f) + Q(f) + H(f), \end{aligned} \tag{2.3}$$

where

C = Coulomb collision term [13, 10, 11, 12],
Q = rf quasilinear diffusion operator [14, 15],
H = synchrotron radiation term [9],
R = model radial diffusion operator given below,
S = particle source/sink, for example, from neutral beam deposition, or ripple loss.

The local FP operator $\nabla_{\underline{u}} \cdot \underline{\Gamma}_{\underline{u}}$ can be written

$$-\nabla_{\underline{u}} \cdot \underline{\Gamma}_{\underline{u}} = \frac{1}{u^2} \frac{\partial G}{\partial u} + \frac{1}{u^2 \sin\theta} \frac{\partial H}{\partial \theta}, \tag{2.4}$$

$$G = -u^2 \Gamma_u \equiv \left(A + B \frac{\partial}{\partial u} + C \frac{\partial}{\partial \theta} \right) f, \tag{2.5}$$

$$H = -u \sin\theta \, \Gamma_\theta \equiv \left(D + E \frac{\partial}{\partial u} + F \frac{\partial}{\partial \theta} \right) f,$$

where Γ_u, Γ_θ are the u, θ components in momentum space of the flux vector $\underline{\Gamma}_{\underline{u}}$; the FP coefficients $A \rightarrow F$ are specific to the processes in Eq. 2.3. In terms of the small parameter $\delta \equiv \rho_{\rm L\,pol}/a$, where $\rho_{\rm L\,pol}$ is gyroradius using the poloidal magnetic field, *i.e.*, $\rho_{\rm L\,pol}$ is the banana width, and a is a representative plasma minor radius, we have [16] in Eq. 2.2

$$\begin{aligned} v_{\rm D} &\sim \delta, \\ \frac{d\mu}{dt} &\sim \delta^2, \\ \frac{d\varepsilon}{dt} &= q E_\parallel \frac{u_\parallel}{\gamma} + O\left(\delta^2\right). \end{aligned}$$

The CQL3D code uses the "zero-banana-width" approximation, *viz.*, $\delta \rightarrow 0$, thus the collisionless guiding center orbits of the particles are assumed to move on a flux surface identified by radial coordinate ρ. In addition, electrostatic potential terms are omitted in this treatment. Thus, the total derivative of f is given by

$$\frac{df}{dt} = \frac{\partial f}{\partial t} + v_\parallel \hat{b} \cdot \nabla f + q E_\parallel v_\parallel \frac{\partial f}{\partial \varepsilon} + O(\delta). \tag{2.6}$$

The partial derivatives in this equation are taken holding five of the six independent variables ε, μ, $\underline{r}$, t constant.

To obtain the bounce-averaged equation, the further ordering $\tau_{\rm b}/\tau_{\rm coll} \ll 1$ is assumed. The lowest order term in Eq. 2.1 is $v_\parallel \hat{b} \cdot \nabla f = v_\parallel \, \partial f / \partial \ell_{\rm B} \sim f/\tau_{\rm b}$, where $\ell_{\rm B}$ is distance along $\underline{B}$. All remaining terms are taken to vary on time scales at least as great as $\tau_{\rm coll}$. Thus, ordering f,

$$f = f_0 + f_1 + \ldots,$$

where $f_i \sim O[(\tau_b/\tau_{coll})^i]$, we obtain

$$v_\parallel \frac{\partial f_0}{\partial \ell_B} = 0, \tag{2.7}$$

$$\frac{\partial f_0}{\partial t} + v_\parallel \frac{\partial f_1}{\partial \ell_B} = -\frac{qE_\parallel}{m}\frac{\partial f_0}{\partial u_\parallel} + \text{RHS}; \tag{2.8}$$

RHS represents the right-hand side of Eq. 2.1.

Equation 2.7 shows that f_0 is independent of distance along the magnetic field line, *viz.*, of poloidal angle on a flux surface since we assume toroidal symmetry, for each region of phase space with velocity $v_\parallel \neq 0$. We assume that there is only one local minimum of the magnetic field on a flux surface; this is the point through which all particles pass. Here, f_0 can be written as a function of $\varepsilon, \mu, \rho, t$. Up-down symmetry of the plasma cross-section about an equatorial midplane is presently assumed, for computational efficiency. These assumptions exclude a complete treatment of flux surface configurations which have multiple trapped-particle regions such as "bean" shaped plasmas, or are not up-down symmetric.

The bounce-averaged equation is obtained from 2.8 by time-integrating over the periodic particle motion, annihilating the second term,

$$\oint d\tau\, v_\parallel \left.\frac{\partial f_1}{\partial \ell_B}\right|_{\varepsilon,\mu,\rho,t} = \oint df_1 = 0, \tag{2.9}$$

to obtain a bounce-averaged equation

$$\frac{\partial f_0}{\partial t} = -\left\langle\left\langle \frac{qE_\parallel}{m}\frac{\partial f_0}{\partial u_\parallel}\right\rangle\right\rangle + \langle\langle \text{RHS}\rangle\rangle, \tag{2.10}$$

where $\langle\langle\ \rangle\rangle$ is the bounce average,

$$\langle\langle(\ )\rangle\rangle \equiv \frac{1}{\tau_B}\oint' d\tau(\ ); \tag{2.11}$$

the partial bounce time τ_B is defined $\tau_B \equiv \oint' d\tau$, $d\tau \equiv d\ell_B/|v_\parallel|$, and the integral $\oint'$ is taken along the particle orbit ($v_\parallel$ varies according to the constants of motion) from the minimum B point on a flux surface (the outer equatorial plane) to the particle turning point for trapped particles, or to the maximum B point at the inner equatorial plane for passing particles. Up-down symmetric flux surfaces are referred to here.

We will evaluate f_0 on a radial array of non-circular flux surfaces which are labeled by the radial variable $\rho \equiv (\Phi/\pi B_{T0})^{1/2}$ [16], where B_{T0} is a representative toroidal magnetic field usually taken to be the vacuum magnetic field at the plasma major radius. At each ρ, f_0 is taken to be a function of the two momentum-space coordinates, u_0 and pitch angle θ_0, evaluated at the outer equatorial plane where the poloidal angle θ_{pol} is zero; the distribution f at other θ_{pol}-locations is obtained using Eq. 2.7 and the constants of motion, *viz.*,

$$f(u,\theta,\rho,\theta_{pol},t) = f_0\left[u_0(u,\theta),\theta_0(u,\theta),\rho,t\right],$$

where $u_0 = u$,

$$\sin^2\theta_0 = \psi^{-1}\sin^2\theta, \tag{2.12}$$

and $\psi \equiv |\underline{B}|(\theta_{\rm pol})/|\underline{B}|_0$, where $|\underline{B}|_0 = |\underline{B}|(\theta_{\rm pol}=0)$ is the minimum magnetic field on a flux surface.

We obtain the bounce-averaged FP equation 2.10 in a conservative form in momentum space, *i.e.*, except for the explicit source term S, we put the RHS of Eq. 2.10 into the form of a divergence of a flux in $\underline{u}_0$-space and in ρ-space. This is desirable from a computational point of view since then we can use a finite difference scheme which exactly conserves the particle density f_0 in $\underline{u}_0$, ρ-space [17]. Consider the number of particles dN which are in the volume element d^3u_0 and are contained in a flux tube along the magnetic field which is of unit cross-sectional area at $\theta_{\rm pol}=0$, $dN = 2\,\tau_{\rm B}\,|v_{\|0}|\,f_0\,d^3u_0$. This expression is evident from physical considerations: $f_0\,d^3u_0$ is the number density at $\theta_{\rm pol}=0$, multiplying by $|v_{\|0}|$ gives the flux of particles into the tube, further multiplying by $2\,\tau_{\rm B}$ accounts for the length of time that "new" particles are fluxing into the tube, *i.e.*, the time interval before particles are being re-counted. The total number of particles in the flux tube, per cross-sectional area, is

$$N = \int d^3\underline{u}_0\,2\,\tau_{\rm B}|v_{\|0}|f_0.$$

None of the RHS-processes in the FP equation Eq. 2.10, except S and R which will be discussed later, change the total number of particles integrated over velocity space in a flux tube. Hence it is clear that the quantity $|v_{\|0}|\,\tau_{\rm B}f_0$ will be an appropriate quantity for which to obtain a conservative FP equation. We denote $\lambda \equiv |v_{\|0}|\tau_{\rm B}$.

The bounce-averaged FP equation can thus be written

$$\frac{\partial}{\partial t}(\lambda f_0) = -\nabla_{\underline{u}_0}\cdot\underline{\Gamma}_{\underline{u}_0} + \langle\langle R\rangle\rangle + \langle\langle S\rangle\rangle\,, \tag{2.13}$$

where the momentum-space divergence is given analogous to Eqs. 2.4 and 2.5,

$$-\nabla_{\underline{u}_0}\cdot\Gamma_{\underline{u}_0} = \frac{1}{u_0^2}\frac{\partial}{\partial u_0}G_0 + \frac{1}{u_0^2\sin\theta_0}\frac{\partial}{\partial\theta_0}H_0, \tag{2.14}$$

$$G_0 \equiv -u_0^2\Gamma_{u_0} = \left(A_0 + B_0\frac{\partial}{\partial u_0} + C_0\frac{\partial}{\partial\theta_0}\right)f_0,$$

$$H_0 \equiv -u_0\sin\theta_0\,\Gamma_{\theta_0} = \left(D_0 + E_0\frac{\partial}{\partial u_0} + F_0\frac{\partial}{\partial\theta_0}\right)f_0. \tag{2.15}$$

In Killeen *et al.* [8] the bounce averages in Eq. 2.10 are performed, referring to Eqs. 2.4 and 2.5, giving the following simple prescription for obtaining the bounce-averaged coefficients in Eqns. 2.14 and 2.15 in terms of the local coefficients in Eqns. 2.4 and 2.5:

$$A_0 = \lambda\,\langle\langle A\rangle\rangle\,, \qquad B_0 = \lambda\,\langle\langle B\rangle\rangle\,,$$

$$
\begin{aligned}
C_0 &= \lambda \left\langle \left\langle \frac{\cos\theta}{\psi^{1/2}\cos\theta_0} C \right\rangle \right\rangle, \qquad D_0 = \lambda \left\langle \left\langle \frac{\cos\theta}{\psi\cos\theta_0} D \right\rangle \right\rangle, \\
E_0 &= \lambda \left\langle \left\langle \frac{\cos\theta}{\psi\cos\theta_0} E \right\rangle \right\rangle, \qquad F_0 = \lambda \left\langle \left\langle \frac{\cos^2\theta}{\psi^{3/2}\cos^2\theta_0} F \right\rangle \right\rangle. \qquad (2.16)
\end{aligned}
$$

We will also make repeated use of the flux surface average $\langle\,\rangle$ of functions of the constants of motion. Denoting the general function by G, the flux surface average is the integral of G over the volume increment between two neighboring flux surfaces labeled by Ψ and $\Psi+\Delta\Psi$, divided by the volume increment. The quantity Ψ is the usual poloidal flux function equal to poloidal flux divided by 2π. Thus, the flux surface average is

$$
\langle G\rangle \equiv \frac{\int\limits_{\Psi\subset\Delta\Psi} G\, d^3\underline{x}}{\int\limits_{\Psi\subset\Delta\Psi} d^3\underline{x}} \qquad (2.17)
$$

with volume element

$$
d^3\underline{x} = R\, d\phi\, \frac{d\Psi}{|\nabla\Psi|} d\ell_{\rm p},
$$

R is major radius, ϕ is toroidal angle, and $\ell_{\rm p}$ is distance measured poloidally on a flux surface. Denoting the magnetic field by $\underline{B} = \underline{B}_\phi + \underline{B}_{\rm p}$ where the poloidal magnetic field magnitude is $B_{\rm p} = |\nabla\Psi|/R$, reduces the flux surface average to the expression [16]

$$
\begin{aligned}
\langle G\rangle &= \oint \frac{d\ell_{\rm p}}{B_{\rm p}} G \Big/ \oint \frac{d\ell_{\rm p}}{B_{\rm p}} \\
&= \oint \frac{d\ell_{\rm B}}{B} G \Big/ \oint \frac{d\ell_{\rm B}}{B}\,. \qquad (2.18)
\end{aligned}
$$

We have used $d\ell_{\rm p}/d\ell_{\rm B} = B_{\rm p}/|\underline{B}|$.

If we let $G = d^3\underline{u}\, g[\underline{u}(\underline{u}_0)]$ with $d^3\underline{u} = \psi |v_{\|0}/v_\|| d^3\underline{u}_0$ in accord with Eqs. 2.12, this gives

$$
\langle G\rangle = d^3\underline{u}_0\, |v_{\|0}|\, \tau_{\rm B}\, g\,[\underline{u}\,(\underline{u}_0)] \Big/ \oint' \frac{d\ell_{\rm B}}{\psi}\,, \qquad (2.19)
$$

where $\oint' d\ell_{\rm B}$ indicated the integral along $\underline{B}$ from the outer to the inner equatorial plane. For example, if $g = f_0$ and integrate over $\underline{u}_0$-space, we obtain the relation between the flux surface average density $\langle n\rangle$ and the above number of particles N in a flux tube $\int d^3\underline{u}_0\, 2\,|v_{\|0}|\tau_{\rm B} f_0$,

$$
\langle n\rangle = N \Big/ \oint (d\ell_{\rm B}/\psi)\,, \qquad (2.20)
$$

where $\oint d\ell_{\rm B}$ is the integral along $\underline{B}$ encircling the plasma once in poloidal angle. In the following section, the flux surface averages will be used in forming source terms in Eq. 2.13.

Chapter 3

BOUNCE-AVERAGE TERMS

In this section, formation of various bounce-averaged terms in the FP equation 2.13 and methods of implementation in the code are discussed.

3.1 DC electric field

The bounce-averaged dc electric field terms are obtained by re-examining the local term appearing in Eq. 2.8 in divergence form, and then applying the procedures indicated in Eq. 2.16. Thus, at given $\theta_{\rm pol}$ on a flux surface, the electric field term can be written

$$\frac{qE_\parallel}{m}\frac{\partial f_0}{\partial u_\parallel} = \nabla_{\underline{u}}\cdot\left[\frac{qE_\parallel}{m} f_0 \left(\cos\theta\hat{u} - \sin\theta\hat{\theta}\right)\right], \tag{3.1}$$

which gives contributions to the respective FP coefficients Eq. 2.5 equal to

$$\begin{aligned} A_E &= \frac{qE_\parallel}{m} u^2\cos\theta, \\ D_E &= -\frac{qE_\parallel}{m} u\sin^2\theta. \end{aligned}$$

The dc electric field is taken to be in the toroidal direction

$$E_\phi = E_0\frac{R_0}{R}, \tag{3.2}$$

where E_0 is the field at the plasma major radius R_0, giving

$$\begin{aligned} E_\parallel &= \underline{E_\phi}\cdot\underline{B}/|\underline{B}| \\ &= \frac{E_0 R_0}{R}\frac{B_\phi}{|\underline{B}|}. \end{aligned} \tag{3.3}$$

Then, with Eqs. 2.16 and 2.12, the bounce-averaged coefficients are

$$A_{E_0} = \frac{\lambda\, qE_0 u_0^2}{m}\left\langle\left\langle\cos\theta\,\frac{E_\parallel}{E_0}\right\rangle\right\rangle,$$

$$D_{E_0} = -\frac{\lambda\, q E_0\, u_0 \sin^2\theta_0}{m\cos\theta_0}\left\langle\left\langle \cos\theta\,\frac{E_\parallel}{E_0}\right\rangle\right\rangle. \tag{3.4}$$

For trapped particles, the $\langle\langle\cos\theta(E_\parallel/E_0)\rangle\rangle$ term which thereby has antisymmetric contributions in θ will be zero. For transitting particles, we find

$$\begin{aligned}\left\langle\left\langle \cos\theta\,\frac{E_\parallel}{E_0}\right\rangle\right\rangle &= \frac{1}{\tau_{\rm B}}\oint'\frac{d\ell_{\rm B}}{|v_\parallel|}\cos\theta\,\frac{R_0}{R}\,\frac{f}{R|\underline{B}|} \\ &= \frac{\mathrm{sgn}(\cos\theta_0)\,\gamma R_0 f}{\tau_{\rm b}\,u_0\,|\underline{B}|}\left\langle\frac{1}{R^2}\right\rangle\oint'\frac{d\ell_{\rm B}}{\psi},\end{aligned} \tag{3.5}$$

where $f = RB_\phi$ is constant on a flux surface [16], and ψ and $|\underline{B}_0|$ are defined following Eq. 2.12. The indicated integrations are carried numerically, and results for Eq. 3.5 used in Eq. 3.2.

3.2 Relativistic collision coefficients

In present day tokamak experiments, relativistic effects on the electrons are frequently of some importance. For example, in lower hybrid or fast wave current drive experiments, the waves are launched with parallel velocity up to ~ 0.9 c. Also, several plasma diagnostics are sensitive to high energy electrons: hard x–ray radiation and electron cyclotron emission detectors measure radiation from electrons at energies up to ~ 500 keV. As described below, CQL3D presently incorporates a model for "mildly relativistic" Coulomb collisions [11, 12], accurate for usual tokamak situations in which the relativistic tail electrons are colliding on a non-relativistic thermal population, *i.e.*, $v_{T_{\rm e}} \ll c$ where $v_{T_{\rm e}} = (T_{\rm e}/m_{\rm e})^{1/2}$ is the electron velocity. (This model is being extended to a fully relativistic collision treatment [18] based on the methods developed by Braams and Karney [10].)

The local collisional FP operator for species a colliding on species b is given by

$$\begin{aligned}\left.\frac{\partial f_a}{\partial t}\right|_c &= -\nabla_{\underline{u}}\cdot\underline{\Gamma}_{\rm c}, \\ \underline{\Gamma}_{\rm c} &= -\frac{2\pi Z_a^2 Z_b^2 e^4 \ln\Lambda_{ab}}{m_a}\sum_b\int M \\ &\quad\cdot\left[\frac{f_b(u')}{m_a}\nabla_{\underline{u}} f_a(\underline{u}) - \frac{f_a(\underline{u})}{m_b}\nabla_{\underline{u}'} f_b(\underline{u}')\right] d^3\underline{u}'.\end{aligned} \tag{3.6}$$

In the case that the primed "field" particles in Eq. 3.6 have momentum-per-mass $u'^2 \ll c^2$, then the familiar non-relativistic dyad is sufficient [11, 12],

$$M = \nabla_{\underline{v}}\nabla_{\underline{v}}\left|\underline{v} - \underline{v}'\right|. \tag{3.7}$$

This gives the following "mildly relativistic" collisional FP coefficients [11, 12],

$$\frac{1}{\Gamma_a}\left.\frac{\partial f_a}{\partial t}\right|_c = \frac{1}{u^2}\frac{\partial \mathscr{G}_a}{\partial u} + \frac{1}{u^2\sin\theta}\frac{\partial \mathscr{H}_a}{\partial\theta}, \tag{3.8}$$

with

$$\begin{aligned}\mathscr{G}_a &= \left\{A_a + B_a \frac{\partial}{\partial u} + C_a \frac{\partial}{\partial \theta}\right\} f_a, \\ \mathscr{H}_a &= \left\{D_a + E_a \frac{\partial}{\partial u} + F_a \frac{\partial}{\partial \theta}\right\} f_a. \end{aligned} \tag{3.9}$$

The local coefficients are

$$\begin{aligned} A_a &= -\frac{1}{2} u^2 \gamma^3 \frac{\partial}{\partial u} \left(\gamma \mathscr{I}_a\right), \\ B_a &= \frac{1}{2} u^2 \gamma^3 \frac{\partial}{\partial u} \left(\gamma^3 \frac{\partial g_a}{\partial u}\right), \\ C_a &= \frac{1}{2} u \gamma^3 \frac{\partial}{\partial u} \left(\frac{\gamma}{u} \frac{\partial g_a}{\partial \theta}\right), \\ D_a &= -\frac{1}{2} \gamma \sin\theta \frac{\partial}{\partial \theta} \left(\gamma \mathscr{I}_a\right), \\ E_a &= \frac{1}{2} u \sin\theta \gamma^3 \frac{\partial}{\partial u} \left(\frac{\gamma}{u} \frac{\partial g_a}{\partial u}\right), \\ F_a &= \frac{1}{2} \sin\theta \left(\frac{\gamma^4}{u} \frac{\partial g_a}{\partial u} + \frac{\gamma^2}{u^2} \frac{\partial g_a}{\partial \theta}\right), \end{aligned} \tag{3.10}$$

with

$$\mathscr{I}_a = \frac{1}{u^2} \frac{\partial}{\partial u} \left(u^2 \gamma^3 \frac{\partial h_a}{\partial u}\right) + \frac{\gamma}{u^2 \sin\theta} \frac{\partial}{\partial \theta} \left(\sin\theta \frac{\partial h_a}{\partial \theta}\right), \tag{3.11}$$

with Rosenbluth potentials in momentum space

$$g_a(\underline{u}) = \sum_b \left(\frac{Z_b}{Z_a}\right)^2 \ln\Lambda_{ab} \int \left|\underline{v} - \underline{v}'\right| f_b\left(\underline{u}'\right) d^3\underline{u}', \tag{3.12}$$

and

$$h_a(\underline{u}) = \sum_b \left(\frac{Z_b}{Z_a}\right)^2 \frac{m_a}{m_b} \ln\Lambda_{ab} \int \frac{\left|\underline{v} - \underline{v}'\right|}{\gamma'} f_b\left(\underline{u}'\right) d^3\underline{u}'. \tag{3.13}$$

In the above, Γ_a and Λ_{ab} are given by

$$\Gamma_a \equiv \frac{4\pi Z_a^4 e^4}{m_a^2},$$

and

$$\ln\Lambda_{ab} \equiv \ln\left\{\left(\frac{m_a M_b}{m_a + m_b}\right) \frac{2\alpha c \lambda_{\mathrm{d}}}{e^2} \max\left[\left(\frac{2E}{m}\right)_{a,b}^{1/2}\right]\right\} - \frac{1}{2},$$

with α the fine structure constant, λ_{d} the Debye length, and E the mean energy of species a or b. The formation of the bounce-averaged coefficients [18] for Eqs. 2.14 and 2.15 follows the methods previously used for the non-relativistic case [1, 8, 19,

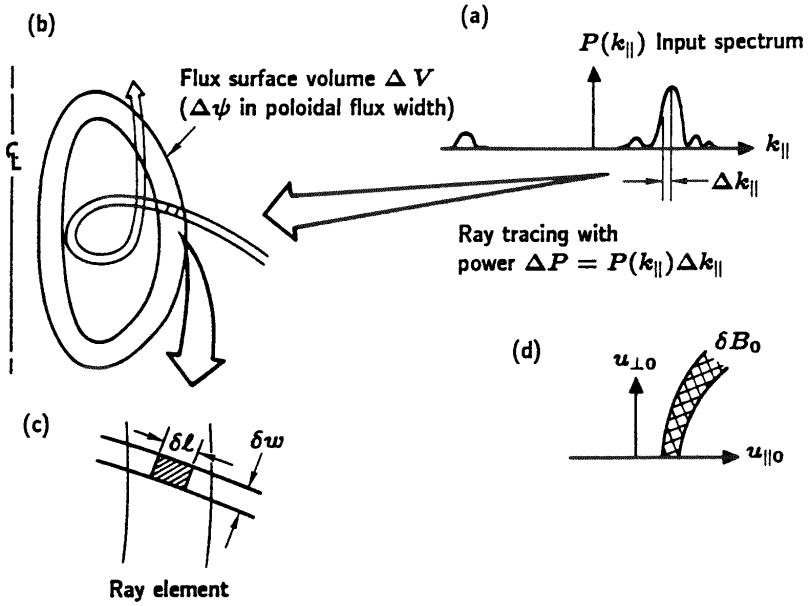

Figure 3.1: *Numerical approach to calculating δB_0 from ray-tracing results.*

20]. Briefly, the angular θ-dependence of the local-in-$\theta_{\rm pol}$ distribution functions and Rosenbluth potentials are expended in Legendre polynomials, and the local coefficients A through F are evaluated at a pitch angle θ such that the particle's orbit traces back to midplane mesh points of θ_0 according to the constraints of motion Eq. 2.12. This eliminates the need for interpolation over a local $u-\theta$ grid during the bounce-average, which thereby reduces to a simple addition.

3.3 The rf quasilinear coefficients

A major use of FP codes has been in modeling of high power rf deposition and consequent quasilinear distortion of ion distributions by ion cyclotron radiation [1, 5, 21, 22], or electron distributions by lower hybrid/fast waves [23, 24] and electron cyclotron waves [20, 25, 26]. In this section we form bounce-averaged FP coefficients based on full expressions for the rf quasilinear operator [14, 15], and we obtain the associated rf damping. The method is applicable for arbitrary wave modes described within the ray-tracing formalism, and for Landau/transit-time and/or cyclotron damping on electrons or ions. Applications have been made to rf interactions with electrons.

The quasilinear diffusion coefficients are obtained based upon rf data passed to CQL3D from a ray-tracing code. As illustrated schematically in Fig. 3.1 [(a) through (d)]: (a) the input power spectrum of rf power $P(k_{\|})$ is obtained, for example, from an antenna code, and is discretized in $k_{\|}$. (b) Consequently, each ray has power $\Delta P = P(k_{\|})\,\Delta k_{\|}$ flowing along it at the launch point. The ray trajectories are calculated using

the linear dispersion relation. (c) The rays are discretized into ray elements of length $\delta\ell$ in the poloidal plane much less than the plasma width. Ray spatial width is taken to be δw, although in the limit of small δw this width will cancel out of the problem. (d) In accord with the finite width $\Delta k_\parallel$ of the power spectrum associated with a ray element, each element contributes a diffusion coefficient (for example, δB) which is non-zero over a region in momentum-per-mass space also of finite width satisfying the wave-particle resonance condition

$$\omega - k_\parallel v_\parallel - n\,\omega_c/\gamma = 0, \tag{3.14}$$

where ω is wave frequency, $k_\parallel$ is a parallel wavenumber in the range of $\Delta k_\parallel$, n is the order of the cyclotron interaction (zero for Landau/transit-time cases), and ω_c is the local cyclotron frequency evaluated with the rest mass. This contributes to the bounce-averaged δB_0. The data passed from the ray-tracing code to CQL3D, for each ray element, includes sufficient information to evaluate the local quasilinear diffusion coefficient, *viz.*, frequency, position, poloidal distance s along the ray, parallel $n_\parallel$ and perpendicular $n_\perp$ refractive index, $n_\parallel$-width $\Delta n_\parallel = c\Delta k_\parallel/\omega$, power in the ray channel $\Delta P(s)$ evaluated from linear damping, rf polarizations $E_x/|E|$, $E_y/|E|$, and $E_z/|E|$ evaluated in the local "Stix" frame [27], energy flux along the ray for electric field strength $|E| = 1$, and the local magnetic field. The resulting contributions to the quasilinear coefficients are used in the calculation of the power absorption for each ray element.

The FP equation is solved on a radial array ρ_i, $i = 1, \ell\rho$ of mesh points. With each point ρ_i, we associate the volume increment ΔV_i between $(\rho_{i-1} + \rho_i)/2$ and $(\rho_i + \rho_{i+1})/2$, except the volume element associated with ρ_1 extends to the plasma magnetic axis and that associated with $\rho_{\ell\rho}$ extends to the plasma edge. The distributions obtained at each radial point ρ_i represent the average over the surrounding volume elements ΔV_i. A ray element contributes to FP coefficients at ρ_i if it falls in volume increment ΔV_i.

Thus the quasilinear coefficients for the bounce-averaged equation can be formed using Eq. 2.16 to relate the bounce-averaged to local quasilinear coefficients, and in addition, an average is performed over volume ΔV_i. Then, the contribution δB_0 to the B_0 coefficient at ρ_i, from each ray element lying in ΔV_i, is

$$\delta B_0 = \frac{1}{\Delta V_i}\int_{\Delta V_i} dV\,\frac{\lambda}{\tau_b}\oint'\frac{d\ell_B}{|v_\parallel|}\,\delta B. \tag{3.15}$$

δB is non-zero only over the spatial volume represented by the ray element, and the momentum space region in which Eq. 3.14 is satisfied.

The remaining coefficients can be similarly evaluated. However the following relations [1] simplify the task: for waves satisfying the wave-particle resonance condition Eq. 3.14, the additional coefficients are related to δB_0 (relativistically) by

$$\begin{aligned}
\delta C_0 &= \frac{1}{u\,\psi\cos\theta_0\sin\theta_0}\left(\frac{n\omega_c}{\omega\gamma} - \psi\sin^2\theta_0\right)\delta B_0,\\
\delta E_0 &= \frac{1}{u\,\psi\cos\theta_0}\left(\frac{n\omega_c}{\omega\gamma} - \psi\sin^2\theta_0\right)\delta B_0,\\
\delta F_0 &= \frac{1}{u^2\,\psi^2\cos^2\theta_0\sin\theta_0}\left(\frac{n\omega_c}{\omega\gamma} - \psi\sin^2\theta_0\right)^2\delta B_0.
\end{aligned} \tag{3.16}$$

The ω_c and ψ are evaluated at the position of the ray element.

In the following subsections we will give an expression for δB, discuss formation of δB_0 from ray element data using Eq. 3.15, and provide specifics of the method as applied to the Landau/transit-time interaction, and the cyclotron interaction.

3.3.1 The δB coefficient

The δB coefficient in the volume represented by the ray element is obtained from the relativistic generalization of the local Kennel and Engelmann [14, 15] expressions,

$$\left.\frac{\partial f}{\partial t}\right|_{q\ell} = \frac{\partial}{\partial \underline{u}} \cdot \left(\underline{\underline{D}}_{q\ell} \cdot \frac{\partial f}{\partial \underline{u}} \right)$$

where

$$\underline{\underline{D}}_{q\ell} = D_{\parallel}\,\hat{u}_{\parallel}\,\hat{u}_{\parallel} + D_{\perp\parallel}\,\hat{u}_{\perp}\,\hat{u}_{\parallel} + D_{\parallel\perp}\,\hat{u}_{\parallel}\,\hat{u}_{\perp} + D_{\perp}\,\hat{u}_{\perp}\,\hat{u}_{\perp}, \tag{3.17}$$

with

$$\begin{aligned}
D_{\parallel} &= \sum_n \frac{q^2}{2m^2}\,\pi\,\delta\left(\omega - k_{\parallel}v_{\parallel} - \frac{n\omega_c^{\pm}}{\gamma}\right)\left|\vartheta^{\pm}_{n,\underline{k}}\right|^2 \cdot \left(\frac{k_{\parallel}u_{\perp}}{\omega\gamma}\right)^2, \\
D_{\parallel\perp} &= D_{\perp\parallel} = \sum_n \frac{q^2}{2m^2}\,\pi\,\delta\left(\omega - k_{\parallel}v_{\parallel} - \frac{n\omega_c^{\pm}}{\gamma}\right)\left|\vartheta^{\pm}_{n,\underline{k}}\right|^2 \left(\frac{k_{\parallel}u_{\perp}}{\omega\gamma}\right)\left(\frac{n\omega_c^{\pm}}{\omega\gamma}\right), \\
D_{\perp} &= \sum_n \frac{q^2}{2m^2}\,\pi\,\delta\left(\omega - k_{\parallel}v_{\parallel} - \frac{n\omega_c^{\pm}}{\gamma}\right)\left|\vartheta^{\pm}_{n,\underline{k}}\right|^2 \cdot \left(\frac{n\omega_c^{\pm}}{\omega\gamma}\right)^2,
\end{aligned} \tag{3.18}$$

and

$$\vartheta^{\pm}_{n,\underline{k}} = J_{n+1}\,\frac{(E_x - iE_y)}{2} + J_{n-1}\,\frac{(E_x + iE_y)}{2} + \frac{u_{\parallel}}{u_{\perp}}\,J_n\,E_{\parallel}. \tag{3.19}$$

$\omega_c^{\pm}$ is the cyclotron frequency with charge sign attached, and $k_{\parallel}$ ($k_{\perp}$) are the wavenumbers parallel (perpendicular) to the ambient magnetic field. The argument of the Bessel functions is $k_{\perp}u_{\perp}/\omega_c^{\pm}$. $\hat{u}_{\parallel}$, $\hat{u}_{\perp}$ are unit vectors in the $u_{\parallel}$ and $u_{\perp}$ directions. The summation in n goes from $-\infty$ to $+\infty$.

The coefficient δB is related to the diffusion coefficient D_{uu} in the u-direction, as is evident from Eqs. 2.4 and 2.5. Thus we must express D_{uu} in terms of the coefficients in Eqs. 3.17 and 3.18. We write

$$\left.\frac{\partial f}{\partial t}\right|_{q\ell} = -\nabla_{\underline{u}} \cdot \underline{\Gamma}_{q\ell}, \tag{3.20}$$

where

$$\underline{-\Gamma}_{q\ell} \equiv \underline{\underline{D}} \cdot \frac{\partial f}{\partial \underline{u}}.$$

Then the fluxes in the $u_{\parallel}$ and $u_{\perp}$ directions are

$$\begin{aligned}
-\Gamma_{u\parallel} &= D_{\parallel}\,\frac{\partial f}{\partial u_{\parallel}} + D_{\parallel\perp}\,\frac{\partial f}{\partial u_{\perp}}, \\
-\Gamma_{u\perp} &= D_{\perp\parallel}\,\frac{\partial f}{\partial u_{\parallel}} + D_{\perp}\,\frac{\partial f}{\partial u_{\perp}},
\end{aligned} \tag{3.21}$$

from which we obtain the flux vector in the u,θ-space,

$$\begin{aligned}\Gamma_u &= \cos\theta\,\Gamma_{u\parallel} + \sin\theta\,\Gamma_{u\perp},\\ \Gamma_\theta &= -\sin\theta\,\Gamma_{u\parallel} + \cos\theta\,\Gamma_{u\perp}.\end{aligned} \tag{3.22}$$

Inserting Γ_u from Eq. 3.22 into 3.20, using 3.21, and transforming the partial derivatives to u,θ-coordinates, then Eqs. 3.18 and 3.19 give the local quasilinear coefficient δB,

$$\delta B = u^2 D_{uu}, \tag{3.23}$$

where

$$\begin{aligned}D_{uu} &= \cos^2\theta\,D_\parallel + 2\cos\theta\,\sin\theta\,D_{\parallel\perp} + \sin^2\theta\,D_\perp\\ &= \sum_n \frac{q^2}{2m^2}\,\pi\,\delta\left(\omega - k_\parallel v_\parallel - \frac{n\omega_c^\pm}{\gamma}\right)\left|\vartheta_{n,k}^\pm\right|^2\left[\cos\theta\,\frac{k_\parallel u_\perp}{\omega\gamma} + \sin\theta\,\frac{n\omega_c^\pm}{\gamma\omega}\right]^2.\end{aligned}$$

The electric field spectrum $\underline{E}_{\underline{k}}$ can be expressed as a function of $k_\parallel$, since the $k_\perp$ is chosen to satisfy the wave dispersion relation. Normalization is such that the root mean square fluctuating electric field is

$$\begin{aligned}E_{\rm rms}^2 &= \int d^3\underline{k}\,\left|\underline{E}_{\underline{k}}\right|^2\\ &= \int_{-\infty}^{+\infty} dk_\parallel\,\left|\underline{E}_{k_\parallel}\right|^2,\end{aligned} \tag{3.24}$$

where $|\underline{E}_{\underline{k}}|^2 = \delta[k_\perp - k_\perp(k_\parallel)]/(2\pi k_\perp)|\underline{E}_{k_\parallel}|^2$. Thus the D_{uu} diffusion coefficient due to a single component $|\underline{E}_{k_\parallel}|^2\Delta k_\parallel$ of the discretized spectrum, representing one of the previously-discussed ray elements, is

$$\begin{aligned}D_{uu} &= \sum_n \frac{\pi q^2}{2m^2}\left[\cos\theta\,\frac{k_\parallel u_\perp}{\gamma\omega} + \sin\theta\,\frac{n\omega_c}{\gamma\omega}\right]^2\frac{\gamma}{|u_\parallel|}\\ &\quad\left|\frac{u_\parallel}{u_\perp}\,J_n\,\frac{E_z}{|E|} + \frac{E_x + iE_y}{2|E|}\,J_{n\mp1} + \frac{E_x - iE_y}{2|E|}\,J_{n\pm1}\right|^2\\ &\quad\left|\underline{E}_{k_\parallel}\right|^2\Delta k_\parallel\,\delta\left(k_\parallel - k_{\parallel\,\rm res}\right),\end{aligned} \tag{3.25}$$

where

$$\delta\left(k_\parallel - k_{\parallel\,\rm res}\right) = \begin{cases}\dfrac{1}{\Delta k_\parallel}, & k_\parallel \subset \Delta k_\parallel,\\ 0, & k_\parallel \not\subset \Delta k_\parallel,\end{cases} \tag{3.26}$$

$$k_{\parallel\,\rm res} = \frac{\omega - n\omega_c/\gamma}{v_\parallel}, \tag{3.27}$$

$\omega_c = |\omega_c^\pm|$, and the argument of the Bessel functions is $k_\perp u_\perp/\omega_c$. The upper signs in the Bessel function indices refer to ions and the lower signs to electrons. We have used $J_{-n}(-z) = J_n(z)$. The summation over n remains from $-\infty$ to $+\infty$.

3.3.2 The δB_0 coefficient

We form the bounce/volume average of δB according to Eq. 3.24, using Eqs. 3.23 and 3.25 through 3.27. We need to relate the power flowing through a ray element to the rf electric field at the ray element. The energy flux flowing in the poloidal plane along a ray is denoted

$$S_{\rm pol} = \frac{\delta P}{\delta w\, 2\pi R} \equiv \tilde{S}_{\rm pol} \left| \underline{E}_{k_\parallel} \right|^2 \Delta k_\parallel . \tag{3.28}$$

$\tilde{S}_{\rm pol}$ is defined as the energy flux [27] in the poloidal plane corresponding to unit $|\underline{E}_{k_\parallel}|^2 \Delta k_\parallel$,

$$\tilde{S}_{\rm pol} = \frac{1}{16\pi} V_{\rm g\,pol} \left[\left| \underline{B}_{k_\parallel} \right|^2 + \underline{E}^*_{k_\parallel} \cdot \frac{\partial(\omega \underline{\underline{K}}_h)}{\partial \omega} \cdot \underline{E}_{k_\parallel} \right] \Big/ \left| \underline{E}_{k_\parallel} \right|^2 , \tag{3.29}$$

$\underline{B}_{k_\parallel} = \underline{n} \times \underline{E}_{k_\parallel}$, $\underline{n} = \underline{k}\, c/\omega$, and $V_{\rm g\,pol}$ is the ray group velocity projected onto the poloidal (*i.e.*, locally meridional) plane. $\tilde{S}_{\rm pol}$ is passed from the ray-tracing code. δP is power flowing in the ray channel of width δw in the poloidal plane (δw is measured perpendicular to $\underline{S}_{\rm pol}$, and it will cancel out of the calculation). The channel may be considered to be toroidally uniform. We also define $\delta \widetilde{B}$ according to

$$\delta B \equiv \delta \widetilde{B} \left| \underline{E}_{k_\parallel} \right|^2 = \frac{\delta \widetilde{B}}{\tilde{S}_{\rm pol}} \frac{\delta P}{2\pi R\, \delta w\, \delta k_\parallel} . \tag{3.30}$$

Then we write

$$\begin{aligned} \int' \frac{d\ell_{\rm B}}{|v_\parallel|}\, \delta B &= \int' \frac{d\ell_{\rm p}}{|v_\parallel|} \left(|\underline{B}| / B_{\rm p} \right) \delta B \\ &\cong \frac{S_{\rm pol}}{S_\Psi}\, \delta w\, \frac{|\underline{B}|}{B_{\rm p}} \left. \frac{\delta B}{|v_\parallel|} \right|_{\substack{u=u_0 \\ \sin^2\theta = \psi \sin^2\theta_0}} , \end{aligned} \tag{3.31}$$

where S_Ψ is flux in $\nabla\Psi$-direction so that $(S_{\rm pol}/S_\Psi)\delta w$ is the poloidal extent of the ray. Forming δB_0 according to Eq. 3.15 gives

$$\begin{aligned} \delta B_0 &= \frac{\int_{\rm ray\,element} R\, d\phi\, d\ell_\Psi\, d\ell_{\rm p}}{\Delta V}\, v_{\parallel 0} \oint' \frac{d\ell_{\rm B}}{|v_\parallel|}\, \delta B \\ &\approx \frac{\delta \ell_\Psi}{\Delta \ell_\Psi}\, v_{\parallel 0} \oint' \frac{d\ell_{\rm B}}{|v_\parallel|}\, \delta B, \end{aligned} \tag{3.32}$$

where $d\ell_\Psi = d\Psi/|\nabla\Psi|$ is a distance increment perpendicular to the flux surface Ψ, $\Delta\ell_\Psi = \Delta\Psi/|\nabla\Psi|$ is the width perpendicular to the flux surface of the volume element ΔV which contains the ray element, $\Delta\Psi$ is the range in Ψ of ΔV, $\delta\ell_\Psi$ is the extent of the ray element in the $\nabla\Psi$ direction,

$$\delta \ell_\Psi = \delta s_{\rm pol} \cdot \frac{S_{\rm pol}}{S_\Psi} , \tag{3.33}$$

and $\delta s_{\rm pol}$ is the ray element length in the poloidal plane. From Eqs. 3.28 through 3.33 and 2.12, we obtain

$$\delta B_0\,(u_0,\theta_0) = \frac{\delta s_{\rm pol}}{2\,\pi\,\Delta\Psi}\,\frac{\cos\theta_0}{\left(1-\psi\,\sin^2\theta_0\right)^{1/2}}\,|\underline{B}|\,\frac{\widetilde{B}}{\tilde{S}_{\rm pol}}\,\frac{\Delta P}{\Delta k_\parallel}. \tag{3.34}$$

The magnetic field $|\underline{B}|$ and ψ are evaluated at $\theta_{\rm pol}$ of the ray, and the coordinates u,θ in $\delta\widetilde{B}$ are evaluated according to Eq. 2.12. This expression is non-zero within narrow strips in u_0,θ_0-space such that the resonance condition Eq. 3.27 has $k_{\parallel\,\rm res}\subset\Delta k$.

Evaluation of the δB_0 for the Landau/transit-time interaction ($n=0$) and the cyclotron damping situations ($n\neq 0$) is essentially identical except for the shape of the resonance strips. We consider these cases separately.

3.3.3 Landau/transit-time interaction ($n=0$)

The resonance strip is defined by the range of parallel refractive index $n_{\parallel 1}\equiv n_{\parallel 0}-\Delta n_\parallel/2$ to $n_{\parallel 2}=n_\parallel 0+\Delta n_\parallel/2$, where $n_{\parallel 0}$ corresponds to the center of the $n_\parallel\equiv k_\parallel c/\omega$-range of a given ray element. The zeroth harmonic ($n=0$) resonance condition, $\omega-k_\parallel v_\parallel=0$, becomes a hyperbola in momentum space at the local $\theta_{\rm pol}$ of the ray element,

$$\left(n_\parallel^2-1\right)\,\frac{u_\parallel^2}{c^2}-\frac{u_\perp^2}{c^2}=1. \tag{3.35}$$

Thus the range of resonance strip ($n_{\parallel 2}>n_{\parallel 1}>1$) is as shown schematically in Fig. 3.2(a). For $n_\parallel\leq 1$, there is no resonance.

The code solves the FP equation on a u_0,θ_0-grid. For each value of $u=u_0$ on the grid, the θ_0-grid values corresponding to values θ in the resonance strip defined in Fig. 3.2(a) are determined, the values of δB_0 are computed according to Eq. 3.34, and the additional quasilinear coefficients are obtained with Eq. 3.16. Values of δB_0 corresponding to θ-grid points for which the surrounding θ-range from $\theta-\delta\theta/2$ to $\theta+\delta\theta/2$ is not entirely in the resonance range, are weighted accordingly; we thus obtain θ_0-grid independence in the limit of small $\Delta n_\parallel$.

The rf power absorption associated with the ray element δP is given by the flux surface average of the power density due to a ray element $\langle\delta P_{\rm RF}\rangle$ multiplied by the value of the flux surface ΔV:

$$\delta P=\langle\delta P_{\rm RF}\rangle\cdot\Delta V,$$

where in accord with Eq. 2.19,

$$\langle\delta P_{\rm RF}\rangle=\int d^3\underline{u}_0\,|v_{\parallel 0}|\,\tau_{\rm B}\,(\gamma_0-1)\,mc^2\,\left.\frac{\partial f_0}{\partial t}\right|_{\rm RF}\Big/\oint'\,d\ell_{\rm B}/\psi\,. \tag{3.36}$$

The term $|v_{\parallel 0}|\tau_{\rm B}\,\partial f_0/\partial t|_{\rm RF}$ is given by Eqs. 2.14 and 2.15 with coefficients given by Eqs. 3.34 and 3.16. The velocity integral over the $\partial/\partial\theta_0\,H_0$-term integrates to zero.

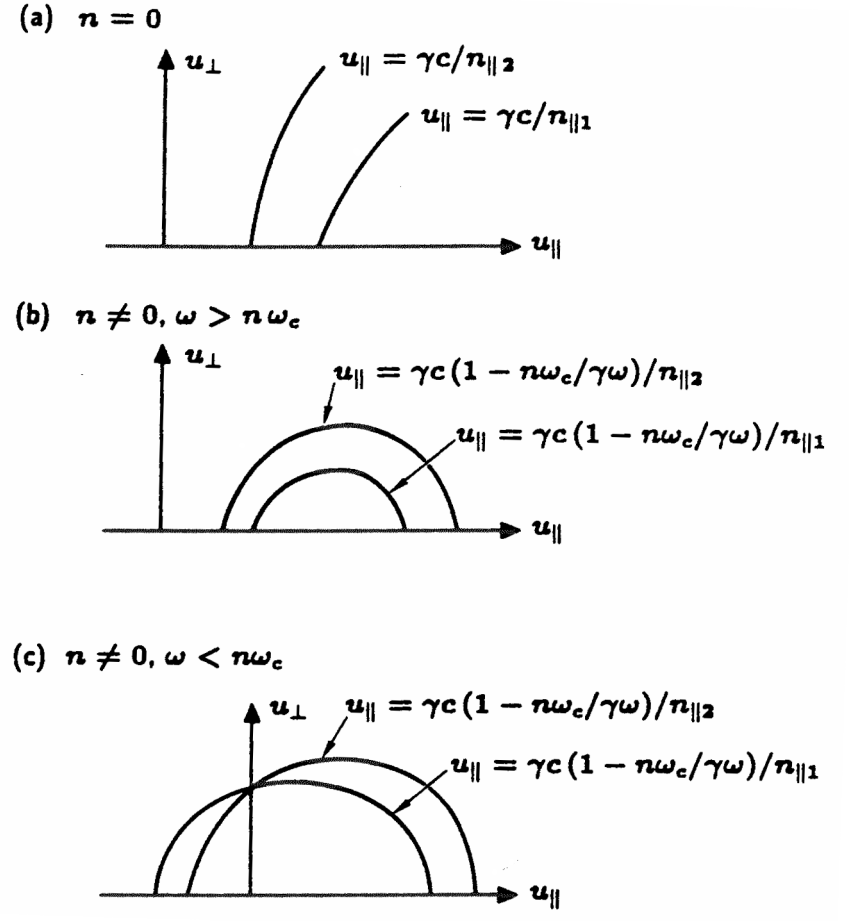

Figure 3.2: *Resonance regions in local momentum-per-mass space are between $n_{\parallel 1}$ and $n_{\parallel 2}$ curves. Three cases are shown: (a) Landau/transit time interaction ($n = 0$), (b) cyclotron interaction with $\omega > n\omega_c$, and (c) cyclotron interaction with $\omega < n\omega_c$.*

3.3.4 Cyclotron interaction $(n \neq 0)$

The resonance strip configurations are more complicated for the $n \neq 0$ cyclotron interactions [26]. Figures 3.2(b) and (c) show the two different situations at the ray element, $\omega \geq n\omega_c$ and $\omega < n\omega_c$. In each case the resonance curve Eq. 3.14 on a specific value of $n_\parallel = k_\parallel c/\omega$ is an ellipse in $u_\parallel, u_\perp$-space:

$$\left(u_\parallel - u_{\parallel 0}\right)^2 + u_\perp^2 / \left(1 - n_\parallel^2\right) = u_0^2, \tag{3.37}$$

where

$$\begin{aligned} \frac{u_{\parallel 0}}{c} &= \frac{n\omega_c}{\omega} \frac{n_\parallel}{1 - n_\parallel^2}, \\ \frac{u_0^2}{c^2} &= \left\{ \left(\frac{n\omega_c}{\omega}\right)^2 - \left(1 - n_\parallel^2\right) \right\} \Big/ \left(1 - n_\parallel^2\right)^2 . \end{aligned}$$

u_0^2 is greater than zero if $(n\omega_c/\omega)^2 > (1 - n_\parallel^2)$. This is an ellipse of ellipticity $(1 - n_\parallel^2)^{-1/2}$. The parallel refractive index of the launched cyclotron waves is less than 1. From Eq. 3.37, the resonance ellipse intercepts the $u_\parallel = 0$ at the two values $u_{\parallel 1}$ and $u_{\parallel 2}$. Figure 3.3 shows schematically the general nature of these intercept values, various values of $n_\parallel$.

Let us first consider the $\omega \geq n\omega_c$-case corresponding to ray elements which are outboard, *i.e.,* on the low magnetic field side, of the resonance surface at $\omega = n\omega_c$. For this case the resonance curves for two neighboring refractive indices $n_{\parallel 1}$ and $n_{\parallel 2}$ do not overlap, as is evident from Fig. 3.3 and shown in Fig. 3.2(b). for each value of u_0 on the mesh, one determines the ray of θ-mesh points (and consequently θ_0-mesh points) which fall into the resonance region in $u_\parallel, u_\perp$-space determined by $n_{\parallel 1}$ and $n_{\parallel 2}$. Again, as in the $n = 0$ case, coefficients are determined according to Eqs. 3.34 and 3.16, and the diffusion coefficients if they are evaluated to θ-points near the edge of the resonance region.

For the $\omega < n\omega_c$ case, as depicted in Figs. 3.2(c) and 3.3, the resonance curves for neighboring $n_\parallel$ overlap. This is not difficult to account for when finding the θ-range for each $u = u_0$, since the curves always overlap at $u_\parallel = 0$, $(u_\perp/c)^2 = (n\omega_c/\omega)^2 - 1$. For u less than this value of $u_\perp$, the order of intersection of the resonance curves with increasing θ is: first, the $k_{\parallel_2}$-curve, then the $k_{\parallel_1}$-curve, assuming $k_{\parallel_2} > k_{\parallel_1} 0$. For greater u, the order of intersection reversed. The treatment is otherwise like the above $\omega > n\omega_c$-case.

The power absorption by cyclotron damping is calculated as above in the manner of the Landau/TTMP interaction, according to Eq. 3.36 with δB_0, etc., given by Eqs. 3.34, 3.16, 3.23, and 3.25.

The code iterates between calculation of the rf quasilinear coefficients, the consistent distorted distribution functions, and the damping of the ray energy along the ray channels, to achieve self-consistent non-Maxwellian distributions and damping of the rf.

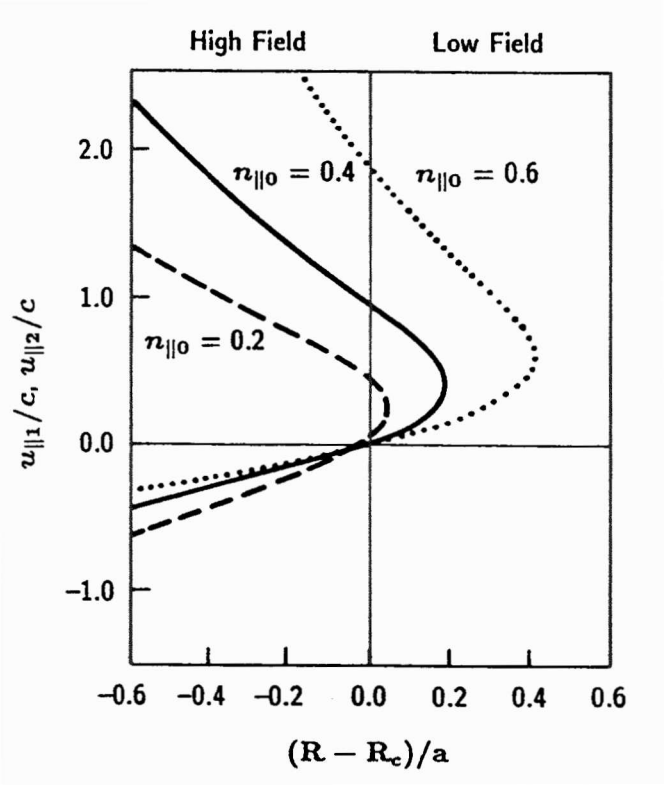

Figure 3.3: *The minimum and maximum $u_{\|}$ on the resonance ellipse ($n \neq 0$) for the cyclotron layer ($\omega = n\omega_c$) at R_c, with the assumption of an R^{-1} variation of the magnetic field. Aspect ratio is 2.5.*

3.4 Bounce-averaged neutral beam source

One of the earliest 2D-in-velocity space, bounce-averaged, finite difference FP codes was FPP, which was constructed by Goldston [28]. Combined with a pencil-beam neutral beam deposition code [28], 2D solutions for the fast ion distribution function were obtained on a radial array of flux surfaces. In the spirit of FPP, CQL3D has been combined with the NFREYA [29, 30] Monte Carlo, neutral beam deposition model, to produce ion distribution functions modified by neutral beam injection (NBI). Running CQL3D in multi-species mode, the NBI driven current can then be calculated directly from the toroidal velocity moments of the ions and the "dragged-along" electrons. In this section, we describe the function of a DIII–D fast ion source, $\langle\langle S\rangle\rangle$ in Eq. 2.13 for ions, from the ion birth points obtained by the Monte Carlo deposition code.

The birth points at given R,Z in the plasma cross-section are statistical in nature. Birth points for each of the particles (subscripted in the following by j), for each of several beam energies, are weighted by a particle source rate W_j which reflects the geometry and physics considerations in the *neutral* beam injection code. The net bounce-averaged source $\langle\langle S\rangle\rangle$ will be the sum of all the individual birth point sources $\langle\langle \delta S_j\rangle\rangle$, weighted by the W_j:

$$\overline{\langle\langle S\rangle\rangle}_{\underline{v}_0} = \sum_j W_j \, \overline{\langle\langle \delta S_j\rangle\rangle}. \tag{3.38}$$

The overbars indicate a further averaging, to be discussed below, over the volume element ΔV_j associated with plasma radius ρ_j and over the computational velocity space increments associated with velocity $\underline{v}_{0j}$. Relativistic effects are ignored.

Suppose a particle is born at poloidal angle $\theta_{\mathrm{p}j}$ on a flux surface Ψ_j, with velocity $\underline{v}_j$. The birth position can also be specified as $\ell_{\mathrm{p}j}$, the poloidal length on the flux surface, and $\ell_{\Psi j}$ which is distance across the flux surface ($d\ell_\Psi \equiv d\Psi/|\nabla\Psi|$). We write δS_j,

$$\delta S_j\,(\underline{r},\underline{v}) = \frac{\delta(\ell_\Psi - \ell_{\Psi j})\,\delta(\ell_\mathrm{p} - \ell_{\mathrm{p}j})}{2\pi R}\,\delta\left(\underline{v} - \underline{v}_j\right), \tag{3.39}$$

such that

$$\int d^3\underline{v} \int d^3\underline{x}\,\delta S_j = 1. \tag{3.40}$$

The source is taken to be toroidally symmetric. Bounce-averaging gives

$$\begin{aligned}
\left\langle\left\langle \delta S_j\right\rangle\right\rangle_{(\underline{v}_0)} &= \frac{1}{\tau_\mathrm{b}(\underline{v}_0,\Psi)} \oint' \frac{d\ell_\mathrm{B}}{|v_\parallel|} \frac{\delta(\ell_\Psi - \ell_{\Psi j})\,\delta(\ell_\mathrm{p} - \ell_{\mathrm{p}j})\,\delta[\underline{v}(\underline{v}_0) - \underline{v}_j]}{2\pi R} \\
&= \frac{|B_0|}{v_{\parallel 0}\tau_\mathrm{B}}\,\delta\left(\Psi - \Psi_j\right) \frac{\delta(v_0 - v_{0j})\,\delta(\eta_0 - \eta_{0j})}{(2\pi)^2 v_0^2},
\end{aligned} \tag{3.41}$$

where $\eta_0 = \cos\theta_0$, and we have used $\delta[\underline{v}(\underline{v}_0) - \underline{v}_j] = \delta(v_0 - v_{0j})\,\delta(\eta_0 - \eta_{0j})/[2\pi v_0^2 \times |(B/B_0)(v_{\parallel 0}/v)|]$, $\delta(\ell_\Psi - \ell_{\Psi j}) = |\nabla\Psi|\,\delta(\Psi - \Psi_j)$, and Eq. 2.12. B_0 is the minimum magnetic field on the flux surface. We further average over the velocity space mesh element that $\underline{v}_0$ falls into, $2\pi v_{0j}^2 \Delta\eta_0 \Delta v_0$, and the volume ΔV_j surrounding the nominal flux surface, giving

$$\overline{\langle\langle \delta S\rangle\rangle}_{\underline{v}_0} = \frac{1}{2\pi v_0^2 \Delta v_0 \Delta\eta_0 \Delta V} \int 2\pi v_0'^2\, dv_0'\, d\eta_0' \int d^3\underline{x}'\,\langle\langle \delta S\rangle\rangle_{\underline{v}_0'}$$

$$= \frac{1}{2\pi v_0^2 \Delta v_0 \Delta\eta_0} \frac{B_0}{2\pi \Delta\Psi v_{\|0} \tau_B}. \tag{3.42}$$

in the v_0-volume element surrounding $\underline{v}_{0j}$ and in ΔV_j, and zero outside. The net source rate is then found using Eq. 3.38.

3.5 Synchrotron radiation

Synchrotron radiation by electrons can be an important energy loss mechanism in a tokamak reactor, particularly in the presence of a nonthermal tail [31, 32]. CQL3D models thus use the bounce-averaged of the local expression given in Ref. [9]. This will give an upper bound on radiation losses, since it omits important effects of wall reflectivity and reabsorption [31, 32].

The local flux in momentum-per-mass space due to synchrotron radiation is

$$\underline{\Gamma}_R = \alpha |\underline{B}|^2 \gamma_\|^2 \left\{ \hat{b} \times \left(\underline{u} \times \hat{b} \right) + \frac{|\hat{b} \times \underline{u}|^2}{\gamma_\|^2 c^2} \left(\hat{b} \cdot \underline{u} \right) \hat{b} \right\} f_e, \tag{3.43}$$

where $\alpha = 2/3\,(e^4/m_e^3 c^5 \gamma)$, $\gamma_\|^2 = 1 + u_\|^2/c^2$, and $\hat{b} = \underline{B}/|\underline{B}|$ is a unit vector parallel to $\underline{B}$. From Eqs. 2.4 and 2.5, Eq. 3.43 gives the advective FP coefficients $A = u^2 \Gamma_u / f_e$ and $D = u \sin\theta \Gamma_\theta / f_e$, where Γ_u, Γ_θ are the components of $\underline{\Gamma}_R$ in the u, θ-coordinate system. This gives

$$\begin{aligned} A &= \alpha |\underline{B}|^2 \gamma_\|^2 u^3 \sin^2\theta \left\{ 1 + \frac{u^2}{\gamma_\|^2 c^2} \cos^2\theta_0 \right\}, \\ D &= \alpha |\underline{B}|^2 \gamma_\|^2 u^2 \sin^2\theta \cos\theta \left\{ 1 - \frac{u^2}{\gamma_\|^2 c^2} \sin^2\theta \right\}. \end{aligned} \tag{3.44}$$

The bounce-averaged coefficients are obtained with Eq. 2.16,

$$A_0 = \alpha \lambda |\underline{B}|_0^2 u^3 \sin^2\theta_0 \left\{ \left(1 + \frac{2u^2}{c^2} \right) \langle\langle \psi^3 \rangle\rangle - \frac{2u^2}{c^2} \sin^2\theta_0 \langle\langle \psi^4 \rangle\rangle \right\}, \tag{3.45}$$

$$\begin{aligned} D_0 = \alpha \lambda |\underline{B}|_0^2 u^2 \frac{\sin^2\theta_0}{\cos\theta_0} \Bigg\{ & \gamma^2 \langle\langle \psi^2 \rangle\rangle - \left(1 + \frac{3u^2}{c^2} \right) \sin^2\theta_0 \langle\langle \psi^3 \rangle\rangle \\ & + 2 \frac{u^2}{c^2} \sin^4\theta_0 \langle\langle \psi^4 \rangle\rangle \Bigg\}. \end{aligned}$$

The bounce averages of ψ^n, which depend on pitch angle θ_0 and radius, are obtained by numerical integration according to Eq. 2.11.

3.6 Simplified lower hybrid diffusion coefficient

The CQL3D code can be run in single flux surface mode. A simplified diffusion operator is available, enabling easy simulation of lower hybrid (LH) current drive and comparison with past 2D FP simulations [23, 24, 33] of this process.

The simplified LH operator, given in terms of a flux in $\underline{u}$-space parallel to the magnetic field, is

$$\underline{\Gamma} = -D_{\parallel} \frac{\partial f}{\partial u_{\parallel}} \hat{u}_{\parallel}, \tag{3.46}$$

where $D_{\parallel}$ is specified. We transfer $\underline{\Gamma}$ to the u, θ-coordinate system and compare with Eqs. 2.4 and 2.5 to obtain the FP coefficient,

$$B = u^2 \cos^2\theta \, D_{\parallel}. \tag{3.47}$$

The coefficient $B_0 = \lambda \langle B \rangle$ for the bounce-averaged equation is formed using a numerical bounce-averaged of B; the remaining nonzero coefficients C_0, E_0, and F_0 are given by Eq. 3.16.

The B-coefficient is specified as a function of $v_{\parallel}$. It is constant and nonzero in the "resonance" region $v_{\parallel 1}$ to $v_{\parallel 2}$, except for a smooth "turn-on" from zero to maximum value, with shape $1/2\,[1-\cos(\pi\left|v_{\parallel}-v_{\parallel \mathrm{i}}\right|/\delta v_{\parallel})]$, i equals 1 and 2, over the interval of width $\delta v_{\parallel}$ at each edge of the resonance region. The diffusion coefficient is specified as a multiplier of the collisional diffusion coefficient $D_{\mathrm{coll}} \equiv v_{T_e^2}/\tau_{\mathrm{ei}}$, $v_{T_e}^2 = T_e/m_e$, $\tau_{\mathrm{ei}} = v_{T_e}^3 m_e^2/(4\pi n_e e^4 \ln\Lambda)$. This gives the value of $D_{\parallel}$ at major radius $R = R_0$, where R_0 is the major radius (center) of a flux surface. The $(v_{\parallel 1}, v_{\parallel 2})$ width of the resonant region is given at R_0 and may be constant over the flux surface, or may vary as R/R_0 thus keeping $k_{\parallel}R$ approximately constant as expected for a lowest order treatment of toroidal effects on the input LH spectrum.

3.7 Radial diffusion operator

Diffusion of electrons, particularly of a fast electron tail in low-density rf current drive experiments, may play an important role in tokamaks. If the radial diffusion coefficient increases with velocity, such as is expected for stochastic magnetic field induced transport, [34], then this effect may significantly limit radial localization of rf current drive. Alternatively, if the radial diffusion effects are more uniform in velocity space, such as may result from a nonresonant $\underline{\tilde{E}} \times \underline{B}$-diffusion, then the effects on tail-electron transport will be less severe. Effects of stochastic magnetic field-induced transport have been previously examined computationally with a 2D, (r, v)-FP code which modeled radial diffusion of a pitch angle-averaged distribution of electrons [35]; application was made to modeling Alcator observations of soft-x–ray tail temperatures which were found to be independent of the X-ray diagnostic tangent radius in the plasma [36]. The present generation of 3D codes [2, 3, 4, 5, 6, 7] examines radial diffusion of the 2D-in-momentum-space distributions.

The radial operator $\langle R \rangle$ in CQL3D contains both a diffusion term $D_{\rho\rho}$ and a convective velocity V_{ρ} term. The V_{ρ} term is chosen to balance the diffusion term so that a

given plasma density profile is maintained. $D_{\rho\rho}$ and V_ρ may be general functions of $\underline{u}$ and ρ, although negative $D_{\rho\rho}$ presumably will present numerical difficulties. The form of $\langle R\rangle$ is chosen to conserve particles. Also, we consider two general categories of radial diffusion: one at constant energy E and magnetic moment μ, following Hammett [5], as may be expected due to nonclassical transport by electromagnetic turbulence at frequencies below the electron cyclotron frequency; and the second at constant equatorial plane pitch angle θ_0 [2, 3], which is somewhat less physically motivated.

We consider the radial transport of the quantity $\lambda f_0/\oint'(d\ell_B/\psi)$ which as discussed previously is the flux surface average of particles in $d^3\underline{u}_0$ at $\theta_{pol}=0$. The operator conserves flux surface average density $\langle n\rangle = \int d^3\underline{u}_0/\oint'(d\ell_B/\psi)$. For noncircular geometry, we obtain

$$\begin{aligned}
\frac{\partial(\lambda f_0)}{\partial t} &= \langle\langle R\rangle\rangle + \ldots, \\
\langle\langle R\rangle\rangle &= \left|\frac{u_{\|0}}{B_0}\right|^{C_0} \frac{\oint' d\ell_B}{H\rho} \left.\frac{\partial}{\partial\rho}\right|_{C_1,C_2} H\rho \left|\frac{B_0}{u_{\|0}}\right|^{C_0} \\
&\quad \cdot \left\{ D_{\rho\rho} \left.\frac{\partial}{\partial\rho}\right|_{C_1,C_2} \left[\frac{\lambda f_0}{\oint'(d\ell_B/\psi)}\right] + V_\rho \frac{\lambda}{\oint'(d\ell_B/\psi)} f_0 \right\},
\end{aligned}$$

where

$$(C_0,C_1,C_2) = \begin{cases} (1,E,u) & \text{for constant } E,\mu \text{ diffusion,} \\ (0,\mu_0,\theta_0) & \text{for constant } u_0,\theta_0 \text{ diffusion.} \end{cases} \tag{3.48}$$

As before, B_0 is the minimum magnetic field on a flux surface. H is a quantity previously used in the ONETWO transport code [37] containing the effects of noncircular geometry [16]; it has the value 1 for circular concentric flux surfaces. The quantity $u_{\|0}/B_0$ appears in the Jacobian of transformation from u_0,θ_0- to E,μ-coordinates, $d^3\underline{u}_0 = |B_0/u_{\|0}|(2\pi\gamma/m^2)dE\,du$. In forming the quantity $\partial\langle n\rangle/\partial t$ by integrating over $d^3\underline{u}_0$, the $u_{0\|}/B_0$ term in Eq. 3.48 enables the interchange of order of integration and differentiation $(\partial/\partial\rho)|_{E,u}$, giving the result that the rate of change of particles between two flux surfaces can be written as the difference between the two boundary surface terms, *i.e.*, the equation is in conservative form.

The numerical implementation of the two different radial derivative forms in Eq. 3.48 is accomplished through the simple artifice of varying the θ_0-grid as a function of radius ρ. For the constant v_0,θ_0-diffusion, the θ_0-grid is constant from flux surface to flux surface, whereas for the constant $E\,\mu$-diffusion, the θ_0-grid is chosen to vary with ρ so as to conserve μ at corresponding θ_0-grid points. Radial derivatives are formed between corresponding θ_0-grid points.

Chapter 4

NUMERICAL SOLUTION OF EQUATIONS AND MODES OF USAGE

CQL3D is a general multispecies, noncircular plasma, time-dependent, nonlinear collisions, radial transport Fokker-Planck code. Generally, not all of the features are used simultaneously due to the complexity of the resulting cases, although its application as a full transport code will likely increase. Here we describe some numerical aspects which pertain to the modes of usage of the code.

Numerical solution of the equations for the 2 D momentum-space time-advancement of the distributions on each radial flux surface is usually performed by a straightforward Guassian elimination of the implicitly-differenced FP equations. The coefficients in the FP equation may be determined from the distribution functions at the beginning of the time-step, or they may be held constant at values in accord with the initial Maxwellian distributions. The method of time-advancement, discussed in Refs. [1], [8], and [19], is usually numerically stable for arbitrary time step δt. If δt is shorter than the time for evolution of the distribution function due to, for example collisions or rf, then the time-evolution of the distributions can be followed. Alternatively, if the FP coefficients are held constant and a steady-state distribution exists, then taking δt longer than the longest time scale in the problem enables a single "time-advancement" step directly to the steady-state solution. Another situation occurs when a steady-state is desired with certain of the FP coefficients evolved consistent with the non-Maxwellian state of the distributions, for example, in rf simulations where the damping of the ray energy depends strongly on distortion of distributions and the FP coefficients must be recomputed for each new state of the ray energy deposition. Then long δt time steps give an iterative approach to the rf steady-state.

As mentioned above, certain of the FP coefficients can be held fixed, depending for example on the initial Maxwellian distribution. This is necessary if a steady-state is desired in cases where there is no radial transport and a heat source is turned on. Otherwise the plasma would heat up indefinitely. In cases of rf or dc electric field in which

the electron distribution is evolved, it is traditional [38, 23, 24] to linearize the electron collisional FP operator by taking the g and h Rosenbluth potentials in Eqs. 3.12 and 3.13 to be entirely due to the initial Maxwellian distributions. A steady-state is achieved whereby added heat from the rf or dc electric field passes mainly to the background Maxwellian "heat bath." This approximation is quite good for cases when only tail electron dynamics are important, and where electron-electron slowing down effects on the tail electrons dominate transport effects, but for situations such as in the calculation of Ohmic conductivity where a significant portion of electron momentum is carried by thermal particles, then the non-conservation of electron momentum during electron-electron collisions implicit in this linearization gives a poor approximation, and leads to a factor $\sim$2.0 reduction in Ohmic conductivity. We have therefore adopted a "partially-nonlinear" mode of operation [33] to prevent the thermal runaway but give momentum conservation in electron-electron collisions: the P_0-Legendre component in the expansion of the evolved electron distribution in Eqs. 3.12 and 3.13 is ignored. Instead we use the P_0-component corresponding to the initial Maxwellian. The remaining P_m-components in Eqs. 3.12 and 3.13 are retained up to a maximum order $m \sim 5$ required for convergence of the results.

If the problem to be solved includes the effects of radial transport, then the code may be run to a steady-state in the "linearized," "partially-nonlinear," or nonlinear modes.

There are several choices of boundary conditions enabling a steady-state in the presence of particle sources or sinks due to, for example, fast ions from neutral beams or electron runaway beyond the maximum energy on the grid. The boundary conditions at the high energy edge of the grid are either zero-flux in momentum-space, or a streaming condition on the distribution permitting a smooth flow of the particles off the edge of the grid. At velocity $v = 0$, the boundary condition can be chosen to be zero-velocity-flux which does not generally permit a steady-state; the distribution can be held fixed at $v = 0$ which leads to a steady-state but the species density may vary from its initial value; or, the distribution can be renormalized to its initial density after each time-advancement step, which leads to a steady-state at the initial density.

Radial transport has been incorporated, building on the previous state of the code in which individual distributions were computed on a radial array of flux surfaces [20, 25] but there was no direct radial coupling of the difference equations. This is readily accomplished by an alternating-direction-implicit (ADI) time advancement scheme [17]:

$$\frac{\lambda\,(f^{n+1/2}-f^{n})}{\delta t/2} = C\left(f^{n+1/2}\right)+Q\left(f^{n+1/2}\right)+S+R(f^{n}), \qquad (4.1)$$

$$\frac{\lambda\,(f^{n+1}-f^{n+1/2})}{\delta t/2} = C\left(f^{n+1/2}\right)+Q\left(f^{n+1/2}\right)+S+R\left(f^{n+1}\right), \qquad (4.2)$$

where f^n represents the distribution function at time step n. Previously we had solved the implicit 2D in momentum-space Eq. 4.1 without R. Adding R in 4.1 amounts to a further source term in this equation. The implicit portion of Eq. 4.2 is 1D in radius and the finite difference equations are readily solved by tridiagonal recursive formulas. We should mention that our first solutions to the full 3D problem utilized a splitting algorithm, which amounted to solving Eq. 4.1 without the explicit $R(f^n)$ term and then

Eq. 4.2 without the explicit $C+Q+S$-term (and with $\delta t/2 \rightarrow \delta t$). Although each step of this scheme was unconditionally stable, short time-steps were required, of order the shortest collision time for the non-Maxwellian portion of the distribution function, in order to avoid oscillations from and momentum- to radial-equation solution. An rf run which took a half-hour of CRAY time without radial diffusion took ten hours to get to steady-state with radial diffusion. Giruzzi found [39] with the slightly more complicated ADI scheme that much longer time steps could be taken, and that in achieving a steady state the radial transport only added a 30% increase in execution time over the rf case with no radial diffusion.

Chapter 5

BENCHMARK RUNS AND ILLUSTRATIVE TRANSPORT CASE

This section outlines three benchmark tests of the code against known results, and gives an example of transport effects on runaway electrons in tokamaks.

5.1 Neutral beam current drive with multispecies operation of code

The NFREYA [36, 37] Monte Carlo neutral beam deposition code was utilized to provide a source of fast ions in an ITER-like plasma [40]. Figure 4(a) shows the tokamak poloidal cross-section, with representative birth points due to three vertically displaced 1.3 MeV deuterium neutral beams injected into a plasma with central electron density $n_{e0} = 1.1 \times 10^{14}$ cm^3. Figure 4(b) gives contours of the resulting steady-state 2D deuterium ion velocity distribution at a point near the plasma center. The electron compensating current due to slowing down of the fast ions on the electrons was computed by two means: (1) running CQL3D in multispecies mode, with both the deuterium and the electrons being simultaneously time-advanced, with no radial transport; the electron current density J_e is then directly calculated by taking the $v_\parallel$-moment in velocity space of the steady-state electron distribution; (2) alternatively, the compensating electron current is obtained from analytic estimates made using formulas by Cordey and Start [41]. Table\:I compares these currents in terms of the fractional reduction of the net beam-driven current density $J_{BD} = J_D + J_e$ divided by the fast ion current density J_D. As a function of inverse aspect ratio, the analytically-obtained current density exceeds the computational result by 1.5% near $\varepsilon \simeq 0.0$ to 6% at $\varepsilon \simeq 0.4$. This good agreement confirms the operation of the electron-ion collision dynamics and trapping effects, with the code working in multispecies mode.

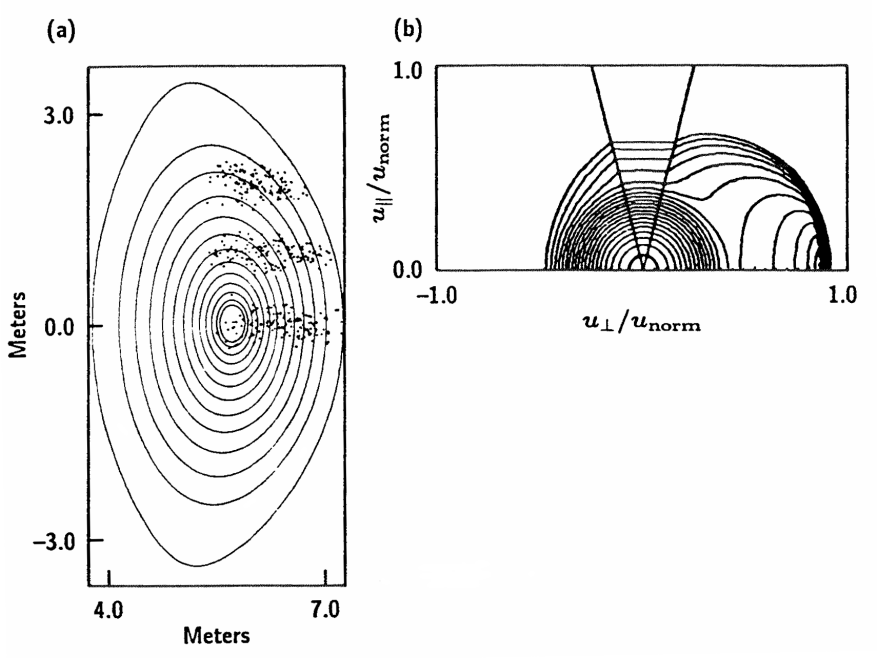

Figure 5.1: (a) Selected birth points of fast ions in ITER-like situation, and (b) the steady-state deuterium distribution at $\rho/a = 0.085$. u_{norm} corresponds to 1800 keV deuterium ions.

Table 5.1:
COMPARISON OF ANALYTIC AND COMPUTATIONAL ESTIMATES OF $J_{\mathrm{BD}}/J_{\mathrm{D}}$

Inverse Aspect Ratio (ε)	Analytic*	Computational
0.0374	0.69	0.68
0.0544	0.73	0.70
0.079	0.76	0.73
0.019	0.79	0.76
0.145	0.82	0.79
0.190	0.86	0.81
0.244	0.88	0.83
0.311	0.90	0.85
0.393	0.93	0.87

*Cordey-Start results, Phys. Fluids **23** (1980) 1475.

5.2 Ohmic resistivity as a function of inverse aspect ratio

Computation of Ohmic resistivity as a function of inverse aspect ratio ε tests the dynamics of electron-ion collisions, momentum conservation properties of electron-electron collisions, and trapping effects, against previous well known banana regime results. The resistivity η in the code is obtained as an area average of the toroidal current density between neighboring flux surfaces, divided by the same average of the electric field E_0 at the plasma major radius, $\eta = \bar{E}_0/\bar{j}$. We ran the code in the previously-discussed "partially-nonlinear" mode. Figure 5 (*cf.*, Ref. [8]) compares the ratio of η normalized to the Spitzer value to several formulas in the literature, both for high and low ε limits. As $\varepsilon \to 0$, the code value of $\eta/\eta_{\text{Spitzer}}$ is 1.03. The code results follow closely the ε variations obtained by Coppi and Sigmar [42] and Connor *et al.* [43] at low ε and by Connor *et al.* [43] at high ε. This further confirms the accuracy of the collision model in CQL3D.

5.3 First harmonic electron cyclotron damping

The present major application of the code is for determination of rf absorption and current drive efficiency. Figure 5.3 compares the damping calculated with CQL3D using relativistic Maxwellian distributions, such as are obtained at low rf power, with results calculated by a linear, relativistic, electron cyclotron wave dispersion code [44]. This is for a case of X–mode radiation launched toward the magnetic axis from the inboard side of a present-day tokamak, at an angle approximately 15 degrees from perpendicular. Data required to calculate the quasilinear diffusion coefficients according to Eqs. 3.23, 3.25, 3.34, and Section 3.3.4 has been passed from the TORAY ray-tracing code [45, 46]. The absorption coefficient giving the damping per unit length along the ray is calculated from the rf power absorption expression Eq. 3.36. The excellent agreement, generally within 3% to 4%, verifies most aspects of rf calculation. The minor numerical difficulty appearing toward the end of the ray trajectory at distance $S \approx 80$ cm occurs near the cyclotron resonance layer $\omega = \omega_c$ in a region where most of the rf power is already absorbed (in this case $\simeq$ 99% absorbed). The difficulty is associated with the first term in square brackets in Eq. 3.25 which together with the resonance condition Eq. 3.27 is proportional to $1/(1-\omega_c/\omega\gamma)^2$.

5.4 Transport effects on runaway electrons

We show results of a typical application of the radial transport model to the problem of electron runaway. Since the slowing down rate for electrons above the thermal energy is proportional to $1/u^3$, eventually an energy is reached where radial transport dominates, since the transport time becomes less than the slowing down time. For densities $\sim 10^{13}/\text{cm}^3$, and assuming a radial transport rate independent of energy, this occurs at energies of order 100 keV for present-day tokamaks. For dc electric field runaway electrons, the only limit on this buildup in the tokamak will be radial transport,

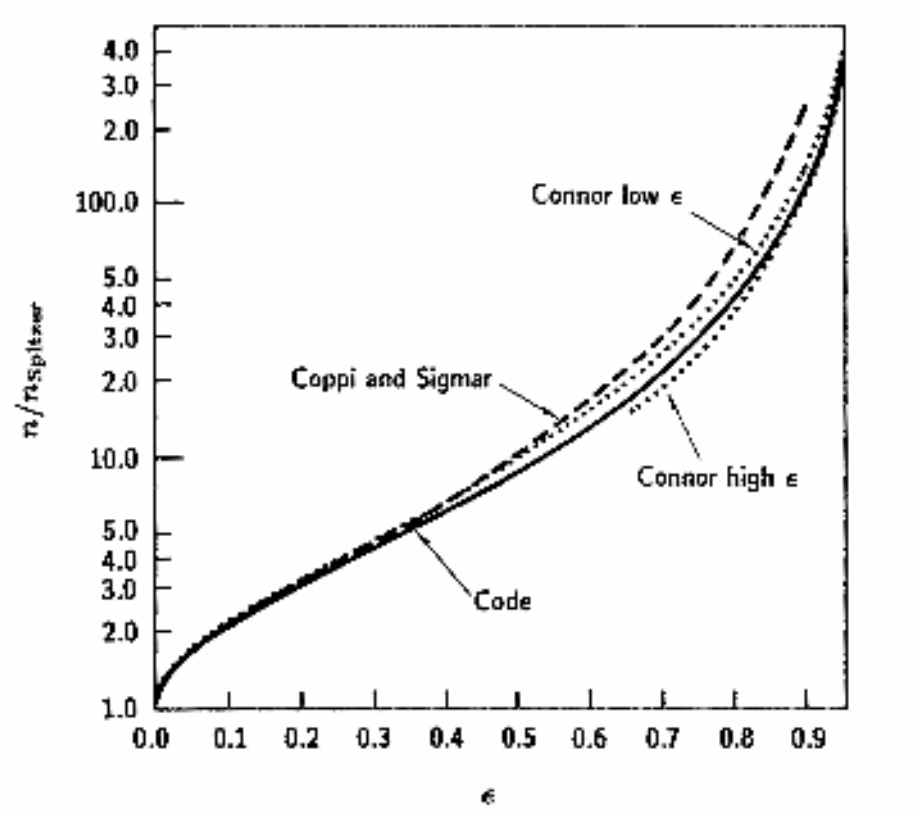

Figure 5.2: *Comparison of Ohmic resistivity* η *from CQL3D to various analytic estimates, as a function of inverse aspect ratio* ε.

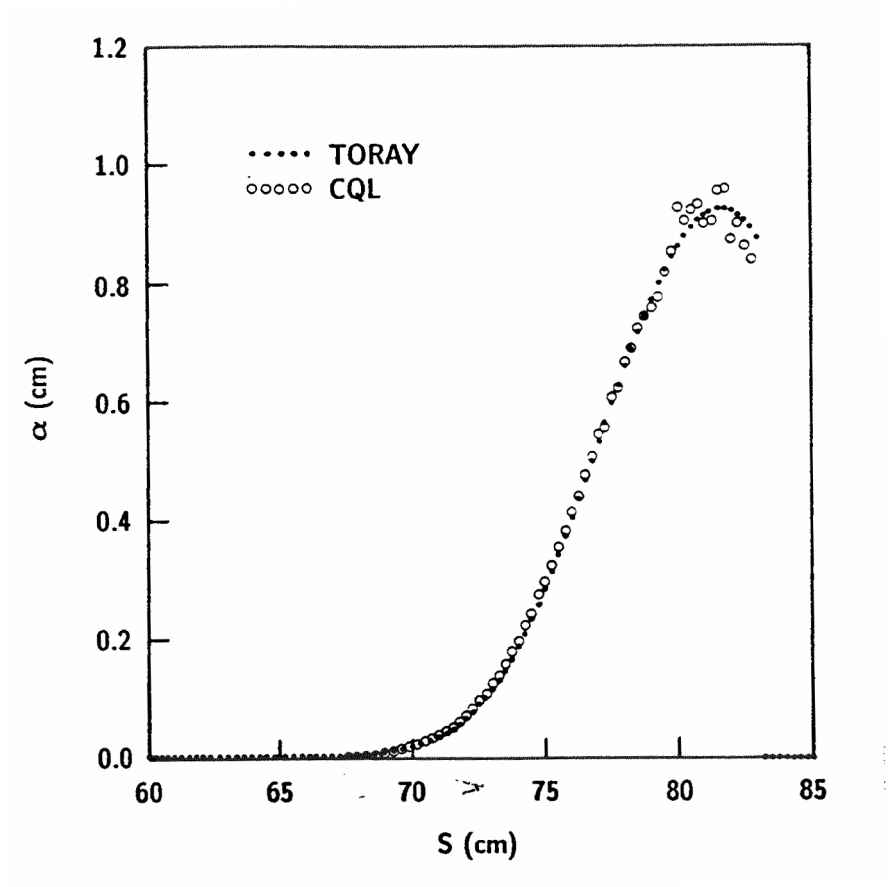

Figure 5.3: *Comparison of electron cyclotron absorption coefficient from CQL3D to results from a relativistic dispersion relation solver [44], as a function of distance along a ray.*

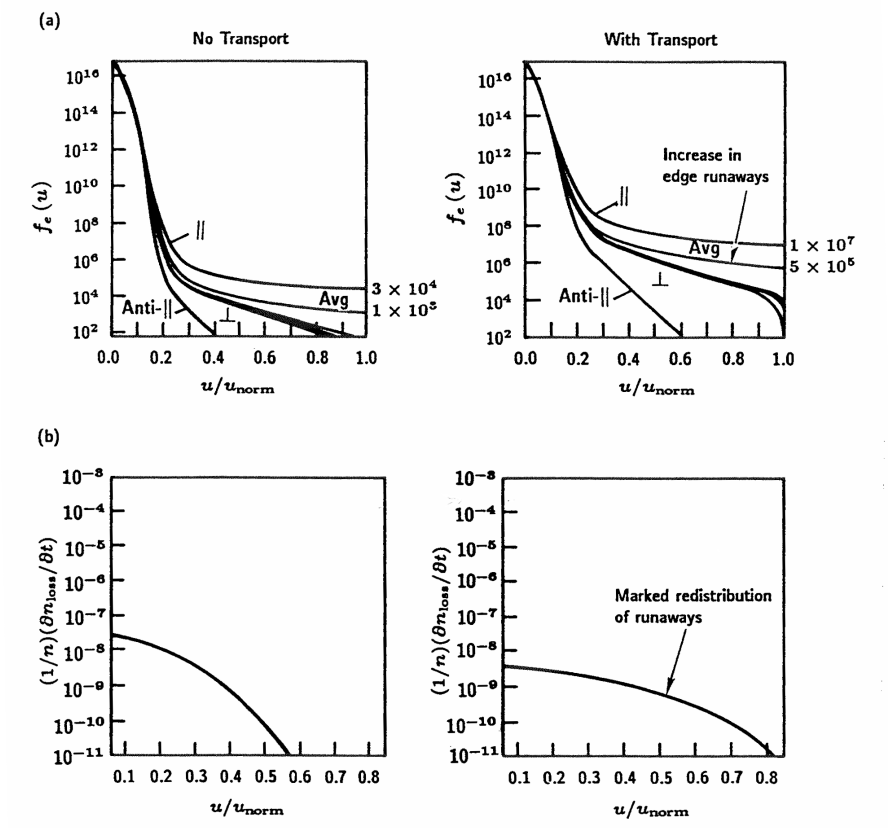

Figure 5.4: *Transport effects of the electron distribution tail, in an Ohmic discharge. Curves on left are for no transport, and curves on right include effects of a radial diffusion transport coefficient* $D_{\rho\rho} = 1.0\ m^2/sec.$ $u_{\rm norm}$ *corresponds to 250 keV electrons.*

or the termination of the discharge. Thus transport effects can be expected to dominate the dynamics of runaways. Figure 5.4 shows results from CQL3D confirming this expectation.

The left hand side of the figure shows results with no radial transport, and the right side is with radial transport. This is for an $n_{e0} = 10^{13}$ cm^{-3}, $Z_{\rm eff} = 1.$, central temperature $T_{e0} = 1$ keV, one-turn voltage $V_\phi = 2.5$ volts, $R_0 = 1.67$ m, Ohmic discharge giving 447 kA current in the "no transport"-case and 428 kA with transport. The diffusion coefficient is a typical value for this type of discharge, $D_{\rho\rho} = 1.0$ m^2/sec, and is independent of velocity. The code is run in the previously discussed "partially nonlinear"-mode, as is appropriate for study of electron tail phenomena.

At the top of Fig. 5.4 we show the electron distributions $f_{\rm e}$ as a function of u, with pitch angle θ_0 as a parameter, at a radius $r/a = 0.65$ toward the plasma periphery. Comparing the left and right of the diagram, we see that transport raises the tail den-

sity by two-and-one-half orders of magnitude, a profound effect on the runaways. The raising of the tail is due to electrons which have transported from the plasma center. The bottom of Fig. 5.4 compares "runaway electron rates," actually the rates of electrons streaming off the edge of the grid above energies 250 keV. As we see, transport depresses these rates at the plasma center, and enhances them toward the plasma edge. Although these transport modifications of the electron tail will have strong effects on tail diagnostics such as x–ray of vertical electron cyclotron measurements, there are not enough tail electrons in this case to significantly modify the current profile.

Chapter 6

CONCLUSIONS

CQL3D is a multispecies, relativistic, 3D bounce-averaged Fokker-Planck code providing a general model for auxiliary heating in tokamaks. We have given an analytic description of each of the terms in the code and outlined how they are numerically implemented. The treatment of the rf quasilinear diffusion and damping terms, which is a new general approach in Fokker-Planck codes, incorporates in a unified fashion the Landau/transit-time and cyclotron interactions of rf energy with the tokamak plasma. A method is given for calculation of fast ion sources from Monte Carlo neutral beam deposition code results.

The CQL3D code has been benchmarked against several known solutions to the Fokker-Planck equations. The Ohmic conductivity agrees within 3 percent with earlier calculations in both the low and high inverse aspect ratio ε limits [41, 42], and provides results in the intermediate ε-regime. This corroborates the electron-electron and electron-ion Coulomb collision terms. A neutral beam injection scenario was set up to obtain the fast ion current; the "dragged along" electron current calculated with the code was compared with analytic expressions [41], giving agreement to 1.5 percent near $\varepsilon = 0.0$ and to 6 percent at $\varepsilon = 0.4$. This validates multispecies use of the code and again the electron-electron and electron-ion collision terms. Electron cyclotron damping on Maxwellian distributions of an electron cyclotron ray was compared with results from a well-known dispersion relation solver [44], and the two results agree generally within 3–4 percent. Since CQL3D calculates rf damping in the same way for non-Maxwellian distributions, and for Landau/transit-time damping, this validates much of the rf quasilinear/damping calculation. An illustrative electron runaway/radial transport simulation demonstrates this functionality in the code and indicates the importance of the radial transport process for high energy electrons.

The code is presently coupled to a range of major auxiliary codes: NFREYA [29, 30] for neutral beam deposition; RAYLH/CURRAY based on Brambilla's lower hybrid tracing code [47] and augmented for general noncircular computational equilibria and fast waves [48]; TORAY [45, 46] and TORCH [49] for electron cyclotron rays; an MHD code for noncircular equilibria; HORACE [50] for electron cyclotron emission consistent with the nonthermal electron distributions; and an internally-calculated x–ray spectrum diagnostic based on the bremsstrahlung emission kernel.

Many generic studies remain to be completed, and new applications can be expected. Future development of the code will focus on incorporation of a self-consistent Ampère-Faraday law for the time-dependent toroidal electric field.

Chapter 7

ACKNOWLEDGMENTS

Gary Kerbel contributed essential elements to the 2D (momentum-space) portion of the code. Mark Franz provided the relativistic version of the collision operator, and upgraded the code accordingly. Gary Smith aided us by providing EC ray data in appropriate format. Martin O'Brien, Y.-R. Lin-Liu, and Olivier Sauter helped us with benchmarking. We gratefully thank John Killeen and Vincent Chan for their support and encouragement. Eric Nelson-Melby has put this document into an editable form (in 2005) and contributed corrections, under the last grant listed below.

This is a report of work sponsored by the U.S. Department of Energy under Contract Nos. DE-AC03-89ER53277, W-7405-ENG-48, and DF-FG02-04ER54744.

Bibliography

[1] KERBEL, G., and McCOY, M., *Phys. Fluids*, **28**, 3629 (1985).

[2] McKENZIE, J., O'BRIEN, M., and COX, M., *Comp. Phys. Commun.*, **66**, 194 (1991).

[3] O'BRIEN, M., COX, M., WARRICK, C., and ZAITSEV, F., "," in *IAEA Technical Committee Meeting on Advances in Simulation and Modeling of Thermonuclear Plasmas*, 1992, (Conference in Montreal, Canada).

[4] GIRUZZI, G., FIDONE, I., and GARBET, X., *Nucl. Fusion*, **32**, 1011 (1992).

[5] HAMMETT, G., *Fast Ion Studies of Ion Cyclotron Heating on the PLT Tokamak*, Ph.D. thesis, Princeton University (1986).

[6] FUKUYAMA, A., and UEEDA, T., "," in *Controlled Fusion and Plasma Heating*, European Physical Society, 1990, vol. 14B, Part III, p. 1251, (Proc. 17th Euro. Conf., Amsterdam, 1990).

[7] SMIRNOV, A. (1992), personal communication.

[8] KILLEEN, J., KERBEL, G., McCOY, M., and MIRIN, A., *Computational Methods for Kinetic Models of Magnetically Confined Plasmas*, Springer-Verlag, New York, 1986.

[9] BERNSTEIN, I., and BAXTER, D., *Phys. Fluids*, **24**, 108 (1981).

[10] BRAAMS, B., and KARNEY, C., *Phys. Fluids*, **1**, 1355 (1989).

[11] FRANZ, M., Tech. rep. (1987), lawrence Livermore National Laboratory Report UCRL-96510.

[12] PEARLSTEIN, D. (1988), personal communication.

[13] ROSENBLUTH, M., MacDONALD, W., and JUDD, D., *Phys. Rev.*, **107**, 1 (1957).

[14] KENNEL, C., and ENGELMANN, F., *Phys. Fluids*, **9**, 2377 (1966).

[15] LERCHE, I., *Phys. Fluids*, **11**, 1720 (1968).

[16] HINTON, F., and HASELTINE, R., *Rev. Mod. Phys.*, **42**, 239 (1976).

[17] RICHTMYER, R., and MORTON, K., *Difference Methods for Initial Value Problems*, Wiley, New York, 1967.

[18] FRANZ, M. (1992), personal communication.

[19] McCOY, M., MIRIN, A., and KILLEEN, J., *Comp. Phys. Commun.*, **24**, 37 (1981).

[20] McCOY, M., KERBEL, G., and HARVEY, R., *Comp. Phys. Commun.*, **40**, 115 (1986).

[21] STIX, T., *Nucl. Fusion*, **15**, 737 (1975).

[22] HARVEY, R., McCOY, M., KERBEL, G., and CHIU, S., *Nucl. Fusion*, **26**, 43 (1986).

[23] KARNEY, C., and FISCH, N., *Phys. Fluids*, **22**, 1817 (1979).

[24] KARNEY, C., *Comp. Phys. Rep.*, **4**, 183 (1983).

[25] HARVEY, R., McCOY, M., and KERBEL, G., "," in *Synopses of 11th Int. Conf. on Numerical Simulation of Plasmas*, Montreal, 1985.

[26] HARVEY, R., McCOY, M., and KERBEL, G., *Phys. Rev. Lett.*, **62**, 426 (1989).

[27] STIX, T., *The Theory of Plasma Waves*, McGraw-Hill, New York, 1962.

[28] GOLDSTON, R. (1980), private communication.

[29] LISTER, G., POST, D., and GOLDSTON, R., "Proc. of 3rd Symp. on Plasma Heating in Toroidal Devices," Varenna, Italy, (Editrice Compositori, Bologna, 1977).

[30] FOWLER, R., HOLMES, J., and ROME, J., Oak ridge national laboratory report ornl/tn-6845, Tech. rep. (1979).

[31] FIDONE, I., GRANATA, G., GIRUZZI, G., and MAZZUCATO, E., *Nucl. Fusion*, **31**, 2167 (1991).

[32] FIDONE, I. (1992), personal communication.

[33] HARVEY, R., MARX, K., and McCOY, M., *Nucl. Fusion*, **21**, 153 (1981).

[34] RECHESTER, A., and ROSENBLUTH, M., *Phys. Rev. Lett.*, **40**, 38 (1978).

[35] HARVEY, R., McCOY, M., HSU, J., and MIRIN, A., *Phys. Rev. Lett.*, **47**, 102 (1981).

[36] MOLVIG, K., RICE, J., and TEKULA, M., *Phys. Rev. Lett.*, **41**, 1240 (1978).

[37] PFEIFFER, W., DAVIDSON, R., MILLER, R., and WALTZ, R., "onetwo, a computer code for modeling plasma transport in tokamaks, Tech. rep., General Atomics Report GA-A16178 (1980).

[38] KULSRUD, R., SUN, Y.-C., WINDSOR, N., and FALLON, H., *Phys. Rev. Lett.*, **31**, 690 (1973).

[39] GIRUZZI, G. (1992), personal communication.

[40] Iter conceptual design: Interim report, Tech. rep., IAEA, Vienna (1990).

[41] CORDEY, J., and START, D., *Phys. Fluids*, **23**, 1475 (1980).

[42] COPPI, B., and SIGMAR, D., *Phys. Fluids*, **16**, 1174 (1973).

[43] CONNOR, J., GRIMM, R., HASTIE, R., and KEEPING, P., *Nucl. Fusion*, **13**, 211 (1973).

[44] MAZZUCATO, E., FIDONE, I., and GRANATA, G., *Phys. Fluids*, **30**, 3745 (1987).

[45] MATSUDA, K., *IEEE Trans. Plasma Sci.* (1989).

[46] KRITZ, A., HUSAN, H., GOLDFINGER, R., and BATCHELOR, D., "," in *Proc. of 3rd Joint Varenna-Grenoble Int. Symp. on Heating in Toroidal Plasmas*, Brussels, 1982, vol. 2, p. 707.

[47] BRAMBILLA, M., *Comp. Phys. Rep.*, **4**, 71 (1986).

[48] MAU, T., CHIU, S., and HARVEY, R., "," in *Proc. Europhys. Top. Conf. on Radiofrequency Heating and Current Drive of Fusion Devices*, European Physical Society, Brussels, 1992, vol. 16E, p. 181.

[49] MEYER, R., et al., *Nucl. Fusion*, **29**, 2155 (1989), (see Appendix).

[50] HARVEY, R., O'BRIEN, M., et al., *Phys. Fluids B*, **5**, 446 (1993).